Spectral reflectance properties of zeolites and remote sensing implications

Edward A. Cloutis,[1] Pranoti M. Asher,[2] and Stanley A. Mertzman[3]

Received 12 February 2001; revised 24 October 2001; accepted 6 June 2002; published 25 September 2002.

[1] The 0.3- to 26-μm reflectance spectra of a suite of 28 zeolites were measured and analyzed to derive spectral-compositional-structural relationships. Below ~7 μm, the spectra are largely dominated by absorption features associated with zeolitic water. At longer wavelengths, the spectra are dominated by absorption features associated with the aluminosilicate framework. The spectra exhibit a number of systematic variations which can be used for both structural and compositional determinations. These include: (1) distinguishing different structural groups on the basis of wavelength position variations associated with absorption features in the 8.5- to 26-μm region that are related to differences in the structure of the aluminosilicate framework; (2) determining the major cation which is present (Ca, Na, K) and the associated electronic environment of the zeolitic water on the basis of how these cations hydrogen bond to the water molecules in the void spaces and consequently affect water-related absorption band positions, particularly in the 1.4, 1.9, and 2.0- to 2.5-μm regions; (3) determining the Al:(Al + Si) ratio and SCFM chemical index on the basis of absorption features in the 7- to 26-μm region which are most sensitive to these compositional variations; and (4) identifying iron-bearing zeolites on the basis of absorption features in the 0.35- to 0.9-μm region. The wavelength position and number of H_2O-associated absorption bands are sensitive to factors such as the type of major cation, degree of hydrogen bonding, and size of the void space, all of which are somewhat interrelated. *INDEX TERMS:* 3934 Mineral Physics: Optical, infrared, and Raman spectroscopy; 5470 Planetology: Solid Surface Planets: Surface materials and properties; 6225 Planetology: Solar System Objects: Mars

Citation: Cloutis, E. A., P. M. Asher, and S. A. Mertzman, Spectral reflectance properties of zeolites and remote sensing implications, *J. Geophys. Res.*, *107*(E9), 5067, doi:10.1029/2000JE001467, 2002.

1. Introduction

[2] Zeolites are an important class of minerals for a wide variety of applications. These include industrial uses such as molecular sieves for ion filtration and separation of a diversity of compounds, as an additive in paper and rubber, and as catalysts for numerous chemical processes [e.g., *Feins and Mullen*, 1970; *Breck*, 1974; *Sand and Mumpton*, 1978; *Tsitsishvili et al.*, 1992]. Zeolites are also petrogenetically important because many of them form under restricted ranges of temperature and/or pressure [e.g., *Coombs et al.*, 1959; *Zen*, 1961; *Breck*, 1974; *Sand and Mumpton*, 1978; *Barrer*, 1982; *Donahoe and Liou*, 1985; *Bowers and Burns*, 1990], and hence are potentially useful indicators of petrogenesis.

[3] Zeolites have been suggested by a number of investigators as being plausibly present on the surface of Mars. There are a number of lines of indirect evidence supporting this contention, including their widespread presence in terrestrial basaltic and volcanic regions [*Barnes et al.*, 1984; *Browne et al.*, 1989; *Zamarreno et al.*, 1989; *Basu et al.*, 1998]. Zeolites also form in cold polar desert environments and are widely present in terrestrial cold desert soils, including those derived from basalts [*Berkley*, 1981; *Berkley and Drake*, 1981; *Gibson et al.*, 1983; *Gibson*, 1985], as well as in the terrestrially weathered portions of Antarctic Martian meteorites [*Gooding*, 1984a, 1984b]. Zeolites may also form through low-temperature gradual alteration (palagonitization) of volcanic ash and tephra [*Bonatti*, 1965; *Hay and Iijima*, 1968; *Geptner*, 1970; *Staudigel and Hart*, 1983; *Zhou and Fyfe*, 1989; *Jercinovic et al.*, 1990], and such a material is assumed to be widely present on the Martian surface [*McSween and Murchie*, 1999; *Johnson et al.*, 1999; *McSween et al.*, 1999; *Bell et al.*, 2000].

[4] While zeolites can form in sedimentary environments [e.g., *Johnsson*, 1990] and possibly, on rare occasions, as primary igneous products [*Luhr and Kyser*, 1989], they are most commonly associated with hydrothermal environments [*Alt et al.*, 1986; *Iijima et al.*, 1984; *Foord et al.*,

[1]Department of Geography, University of Winnipeg, Winnipeg, Manitoba, Canada.
[2]Department of Geology and Geography, Georgia Southern University, Statesboro, Georgia, USA.
[3]Department of Geosciences, Franklin and Marshall College, Lancaster, Pennsylvania, USA.

0148-0227/02/2000JE001467

1986], including hydrothermally altered impact melt rocks and breccias [e.g., *Allen et al.*, 1982; *Golden et al.*, 1992; *Beiersdorfer and Ming*, 1996]. This is significant because impact cratering and hydrothermal alteration are, respectively, important known and inferred surface modification processes on Mars [e.g., *Carr*, 1996]. Zeolites can apparently form very quickly under appropriate hydrothermal conditions [*Browne et al.*, 1989].

[5] Other, less direct lines of evidence also suggest that zeolites may be present on the Martian surface. These include models of Martian weathering history and geological evolution [e.g., *Basu et al.*, 1998], and the behavior of the Martian atmosphere [e.g., *Gooding*, 1986]. As zeolites are able to incorporate large amounts of volatiles, such as CO_2 and H_2O into their structure, they could be an important sink for a variety of Martian volatiles [*Gooding*, 1985; *Ming and Gooding*, 1988; *Jakes and Rajmon*, 1998]. Hence, detection of zeolites on Mars and determination of volatile contents and species would have important implications for reconstructing the planet's geological history, the evolution of its atmosphere, and fate of its inventory of volatiles [e.g., *Carr*, 1996].

[6] The current study focused on Na-, Ca-, and K-bearing zeolites. The 0.3- to 26-μm spectral reflectance properties of 28 zeolites, comprising 15 species, were examined in conjunction with compositional and structural information to determine the coupling between spectral variations, composition, and structure of this class of minerals. The goal was to determine which compositional and structural properties might be amenable to spectral analysis, allowing individual zeolites and zeolite structural and compositional groups to be spectrally distinguished from each other and from other minerals.

2. Structure, Composition, and Petrogenetic Significance of Zeolites

[7] The zeolite class of minerals includes a number of naturally occurring and synthetic species. Zeolites are characterized by an aluminosilicate three-dimensional framework [e.g., *Deer et al.*, 1963] with different spatial arrangements of SiO_4 and AlO_4 tetrahedra. Individual zeolite minerals are distinguished on the basis of this spatial arrangement as well as their major cations and actual or potential volatile contents. We have adopted the classification of *Breck* [1974], who has subdivided zeolites into seven groups based on the specific array of (Al, Si)O_4 tetrahedra. Of these seven groups, six are represented by naturally occurring zeolites (group 3 contains only synthetic members). This structural classification was selected for the present study because of the close correspondence between structure and spectral properties for many minerals; it also accounts for other important properties such as void volumes and spatial arrangement of void spaces, cation exchange properties, and adsorption characteristics. At least two representatives from each of these six groups were included in this study.

[8] Zeolites are important minerals from the perspective of petrogenesis because many form under restricted conditions of pressure and/or temperature, and they have long been used to constrain petrogenetic conditions. The commonly cited "zeolite facies" is one manifestation of their petrogenetic usefulness [e.g., *Coombs et al.*, 1959; *Zen*, 1961]. Some of the formation conditions for the specific zeolites included in this study are summarized below (by structural groups as detailed by *Breck* [1974]). A more detailed discussion of zeolite formation conditions is given by *Barrer* [1982].

[9] The group 1 zeolites which were included in this study (wairakite, gismondine, laumontite, and phillipsite) are composed of single 4-ring (Al, $Si)_4O_8$ units in various configurations (referred to as secondary building units). Differences between group 1 zeolites arise from the type of major cation present and the arrangement of the secondary building units [*Breck*, 1974]. The structural properties of these minerals are somewhat diverse; for example, laumontite contains both 4-, 6-, and 10-ring secondary building units. This group is also diverse in terms of the sites in which water molecules reside and the stability of the structure when subjected to dehydration [*Breck*, 1974].

[10] Wairakite generally forms at temperatures ranging between 60° and 300°C and at depths from 72 to 1600 m. Most wairakite forms at temperatures above 175°C (higher than most zeolites) although it has been reported to crystallize at surface temperatures [*Kristmannsdottir and Tomasson*, 1978]. Data from geothermal wells that pass through olivine basalt in Iceland indicate that gismondine crystallizes between 80° and 90°C [*Kristmannsdottir and Tomasson*, 1978]. The geobarometric conditions of formation for this mineral are not known. Laumontite has been considered an indicator mineral for high-temperature, depth zonation of zeolites in burial diagenesis, although it has also been found to form at very low temperatures [*McCulloh et al.*, 1981]. Laumontite is very difficult to synthesize in the laboratory, requiring temperatures of 250°C and 1000 bars pressure [*McCulloh et al.*, 1981]. Data from geothermal wells in basalt in Iceland indicate that laumontite crystallizes at temperatures between 98° and 230°C [*Kristmannsdottir and Tomasson*, 1978]. Laumontite is encountered in rhyolite, at temperatures from 140° to 200°C, in boreholes in Yellowstone National Park, Wyoming [*Bargar and Beeson*, 1981; *Bargar et al.*, 1981]. Data from geothermal wells in basalt in Iceland show that phillipsite crystallizes between 65° and 85°C [*Kristmannsdottir and Tomasson*, 1978].

[11] Group 2 zeolites consist of single 6-ring (Al, $Si)_6O_{12}$ secondary building units in various configurations [*Breck*, 1974]. The only group 2 zeolite included in this study was erionite. It is found in drill cores from rhyolite-derived sediments in geyser basins in Yellowstone National Park, and crystallized at a temperature below 110°C [*Honda and Muffler*, 1970]. Data from geothermal wells passing through olivine basalt in Iceland indicate that levyne (which commonly precedes erionite) crystallized in the temperature range from 55° to 70°C [*Kristmannsdottir and Tomasson*, 1978].

[12] Group 4 zeolites consist of double 6-ring (Al, $Si)_{12}O_{24}$ secondary building units in various configurations [*Breck*, 1974]. Chabazite was the only group 4 zeolite included in this study. Data from geothermal wells in basalt in Iceland show that chabazite crystallizes at depths from 50 to 400 m and at temperatures from 55° to 75°C [*Kristmannsdottir and Tomasson*, 1978].

[13] Group 5 zeolites consist of complex 4-1, T_5O_{10} secondary building units in various configurations [*Breck*,

1974]. The group 5 zeolites in this study included natrolite, mesolite, scolecite, and thomsonite. Although natrolite has not been found in active geothermal wells, it should crystallize at temperatures similar to mesolite and scolecite, which are found in geothermal wells in basalt in Iceland, at depths from 450 to 1200 m and at temperatures from 70° to 100°C [*Kristmannsdottir and Tomasson*, 1978]. Liquid inclusions in calcite, found with natrolite on the Keweenaw Peninsula, Michigan, indicate that natrolite crystallized at 133°C [*Stoiber and Davidson*, 1959]. Data from geothermal wells in basalt in Iceland show that mesolite and scolecite both crystallize at depths from 450 to 1200 m and between 70° to 100°C, and thomsonite crystallizes at depths from 100 to 550 m and at temperatures from 65° to 110°C [*Kristmannsdottir and Tomasson*, 1978].

[14] Group 6 zeolites consist of complex 5-1, T_8O_{16} secondary building units in various configurations [*Breck*, 1974]. The only group 6 zeolite included in this study was mordenite. In Iceland, mordenite is found in basalt, tuffaceous breccia, and dolerite at temperatures from 75° to 280°C and at depths from 25 to 1800 m [*Kristmannsdottir and Tomasson*, 1978]. In the Katayama geothermal area in Japan, mordenite occurs at temperatures from 60° to 140°C [*Seki et al.*, 1969]. In New Zealand, mordenite is found in rhyolite at depths from 118 to 514 m and at temperatures from 60° to 170°C in the Ohaki-Broadlands geothermal area [*Browne and Ellis*, 1970]. It has also been found in pumice and rhyolite tuff taken at depths from 80 to 213 m and at temperatures from 60° to 164°C, in the Wairakei geothermal area [*Steiner*, 1953].

[15] Group 7 zeolites consist of complex 4-4-1, $T_{10}O_{20}$ secondary building units in various configurations [*Breck*, 1974]. The group 7 zeolites in this study include stilbite, clinoptilolite, heulandite, and stellerite. Data from geothermal wells in basalt in Iceland show that stilbite crystallizes at depths from 45 to 1200 m and at temperatures from 75° to 200°C [*Kristmannsdottir and Tomasson*, 1978]. Clinoptilolite occurs at depths less than 600 m and at temperatures less than 34°C [*Boles*, 1981]. Data from geothermal wells in basalt in Iceland show heulandite crystallizes at depths from 30 to 1200 m and between 65° to 200°C [*Kristmannsdottir and Tomasson*, 1978]. Stellerite is stable to dehydration in a vacuum up to 250°C [*Breck*, 1974].

3. Experimental Procedure

[16] A total of 28 zeolite samples, encompassing 15 different species, were included in this study (Table 1). The samples were crushed by hand in an alumina mortar and pestle and dry sieved to obtain a <45 μm fraction for spectral and compositional analysis. Impurities were removed through a combination of visual inspection with a binocular microscope and with a hand magnet during crushing. Some of the samples were also characterized by powder X-ray diffraction to confirm their identities and to determine whether impurities were present in the samples [*Mertzman*, 2000].

[17] The samples were characterized using X ray fluorescence for major elements [*Mertzman*, 2000] and by instrumental neutron activation analysis (INAA) for selected major elements and minor elements. Ferrous iron was determined using a modification of the procedure outlined by *Reichen and Fahey* [1962]. Ferric iron concentration was taken as the difference between total and ferrous iron. Volatile contents (expressed as loss on ignition in Table 1) were determined by heating splits of the samples to 950°C for 1 hour and measuring the associated weight loss. Sample descriptions, selected major element abundances and volatile content (measured as loss on ignition) are provided in Table 1. Elemental abundances were determined for the volatile-free samples after loss on ignition was measured.

[18] Reflectance spectra for the <45 μm-size fractions were measured at the NASA-supported RELAB spectrometer facility at Brown University. The samples were measured at i = 30° and e = 0° relative to halon for the 0.3- to 2.6-μm region at 5 nm spectral resolution and at i = 30° and e = 30° with 4 cm^{-1} spectral resolution relative to brushed gold for the 2.5- to 26-μm region. The 0.3- to 2.6-μm spectra were measured under ambient atmosphere. The 2.5- to 26-μm spectra were measured after purging the samples (removal of water and CO_2) for at least 5 hours. Consequently, the 0.3- to 2.5-μm spectra may exhibit spectral features associated with adsorbed water. Details of the RELAB facility and spectral acquisition procedures is given by *Pieters* [1983] and *Reflectance Experiment Laboratory* [1996]. The spectra were merged at 2.5 μm by multiplying the longer wavelength spectrum by an appropriate correction factor calculated in the region of spectral overlap (2.5–2.6 μm). Absorption band depths were calculated using equation (32) of *Clark and Roush* [1984].

4. Overview of Spectra

[19] The spectral properties of zeolites, both in reflectance and transmittance, have been measured by a number of investigators. The 0.3- to 26-μm reflectance spectra of a number of zeolites are shown in Figure 1. The spectra are broadly similar in nature and are characterized by a number of absorption bands and generally decreasing reflectance toward longer wavelengths.

4.1. Group 1 Zeolites

[20] Compositionally the two wairakite samples are very diverse (Table 1). ZEO105 differs significantly from the ideal formula and that determined for a wairakite from Wairakei, New Zealand [*Deer et al.*, 1963] containing significantly more Si and less Ca. The XRD data indicate that ZEO105 contains both wairakite and quartz. The gismondine, phillipsite and one of the laumontite (ZEO119) samples are compatible with previous compositional determinations and the ideal formulas. The other laumontite sample (ZEO120) contains appreciably more Ca than expected. XRD analysis of this sample indicates that it contains both laumontite and calcite; the presence of calcite would account for the higher-than-expected calcium content.

[21] The spectrum of the <45-μm fraction of gismondine is shown in Figure 1. All of the group 1 spectra are characterized by high reflectance in the visible region, >70% at 0.5-μm in all cases. The 0.3- to 3.3-μm spectra are dominated by absorption features in the 1.4, 1.9, and 2.8-μm regions, associated with zeolitic water as discussed below. The absorption features in these regions vary in detail between different minerals. They also exhibit one or two absorption features in the 2.5- to 2.6-μm region as

Table 1. Analytical Data for Zeolite Samples[a]

Sample ID[b]	ZEO105	ZEO106	ZEO107	ZEO108	ZEO109	ZEO110	ZEO111
MNMH ID[c]	137255	143354	85160	138649	46267–1	83259	93085
Structural group[d]	1	1	1	1	5	5	5
SiO_2	82.04	59.59	46.85	45.36	51.22	46.85	53.63
TiO_2	0.14	0.06	0.00	0.01	0.00	0.00	0.00
Al_2O_3	10.11	25.14	33.06	33.65	31.00	33.01	29.98
FeO	0.29	–	–	–	–	–	–
Fe_2O_3	0.73	0.91[e]	0.21[e]	0.33[e]	0.18[e]	0.12[e]	0.11[e]
MnO	0.029	0.022	0.007	0.008	0.006	0.005	0.005
MgO	0.29	0.22	0.06	0.134	0.084	0.049	0.041
CaO	3.20	13.35	15.28	15.56	11.24	12.32	16.28
Na_2O	0.151	0.392	0.443	0.45	6.82	6.83	0.24
K_2O	2.484	0.015	3.506	2.39	0.009	0.020	0.016
P_2O_5	0.030	0.021	0.011	0.019	0.007	0.010	0.007
Sr	80	109	3124	12174	555	3401	90
Zr	98	38	54	<2	30	7	40
V	47	40	35	38	33	32	33
Cr	41	36	39	34	31	33	38
Total[f]	99.52	99.75	99.81	99.36	100.65	99.63	100.34
LOI[g]	2.59	9.01	20.32	21.33	13.13	12.82	14.12
Al:(Al + Si)	12.3	32.1	44.5	45.7	40.7	42.1	38.8
SCFM[h]	0.96	0.80	0.75	0.74	0.82	0.79	0.77

Sample ID[i]	ZEO112	ZEO113	ZEO114	ZEO115	ZEO116	ZEO117	ZEO118
MNMH ID[c]	R4303-1	113929	94550	106928	162474	112868	R4175
Structural group[d]	7	5	5	5	5	4	4
SiO_2	68.46	51.61	52.12	52.71	50.08	65.30	64.38
TiO_2	0.00	0.00	0.00	0.00	0.01	0.37	0.00
Al_2O_3	19.43	29.35	29.67	29.04	30.25	18.17	22.30
FeO	–	–	–	–	–	0.28	–
Fe_2O_3	0.11[e]	0.10[e]	0.25[e]	0.20[e]	0.11[e]	1.97	0.14[e]
MnO	0.004	0.005	0.005	0.010	0.005	0.038	0.013
MgO	0.087	0.134	0.058	0.110	0.051	3.051	0.094
CaO	10.39	10.24	11.05	0.97	1.56	3.40	10.18
Na_2O	1.23	8.14	6.68	17.34	0.040	1.879	1.460
P_2O_5	0.006	0.008	0.007	0.007	0.009	0.090	0.007
Sr	77	95	72	115	10201	681	6404
Zr	31	44	49	36	<2	173	<2
V	36	37	33	34	30	69	32
Cr	30	35	34	122	35	48	33
Total[f]	99.77	99.73	99.89	100.47	100.16	99.49	100.11
LOI[g]	18.94	13.38	13.00	10.27	10.29	18.39	27.19
Al:(Al + Si)	24.4	39.3	39.3	38.5	40.7	24.0	28.2
SCFM[h]	0.87	0.83	0.82	0.98	0.97	0.91	0.86

Sample ID[j]	ZEO119	ZEO120	ZEO121	ZEO122	ZEO123	ZEO124	ZEO125
MNMH ID[c]	85382	97504	132753	104654	122858	121217	122860
Structural group[d]	1	1	7	7	1	1	2
SiO_2	65.93	38.09	68.04	67.41	65.35	66.24	70.46
TiO_2	0.00	0.00	0.00	0.00	0.18	0.66	0.52
Al_2O_3	21.30	15.72	20.12	20.76	18.54	18.77	14.81
FeO	–	–	–	–	0.22	0.24	–
Fe_2O_3	0.18[e]	0.16[e]	0.13[e]	0.09[e]	1.92	1.85	3.05[e]
MnO	0.008	0.232	0.006	0.004	0.009	0.018	0.034
MgO	0.225	0.435	0.077	0.028	0.289	1.777	1.069
CaO	10.61	43.47	7.20	9.71	0.31	4.79	0.99
Na_2O	1.10	0.32	3.76	2.09	9.18	1.30	5.20
K_2O	0.290	0.929	1.062	0.035	4.235	3.471	4.099
P_2O_5	0.008	0.031	0.008	0.011	0.071	0.064	0.057
Sr	218	236	723	101	65	2230	287
Zr	23	16	25	23	200	703	577
V	31	36	37	35	60	79	145
Cr	47	38	35	35	39	67	39
Total[f]	99.69	99.43	100.50	100.16	100.35	99.57	100.43
LOI[g]	17.24	26.38	17.60	18.71	16.68	15.02	10.94
Al:(Al + Si)	26.8	31.9	25.1	25.9	24.4	24.4	19.3

Table 1. (continued)

Sample ID[j]	ZEO119	ZEO120	ZEO121	ZEO122	ZEO123	ZEO124	ZEO125
MNMH ID[c]	85382	97504	132753	104654	122858	121217	122860
Structural group[d]	1	1	7	7	1	1	2
SCFM[h]	0.86	0.46	0.90	0.87	0.99	0.91	0.97
Sample ID[k]	ZEO126	ZEO127	ZEO128	ZEO129	ZEO130	ZEO131	ZEO132
MNMH ID[c]	122847	144077	114104-1	122861	122848	R4073-1	138663
Structural group[d]	2	7	7	6	6	7	7
SiO_2	70.25	73.80	77.37	71.96	64.66	66.46	69.42
TiO_2	0.32	0.30	0.06	0.68	0.54	0.00	0.00
Al_2O_3	15.97	13.22	13.53	14.42	10.00	19.78	19.18
FeO	–	0.24	–	–	–	–	–
Fe_2O_3	2.37[e]	3.01	0.48[e]	1.93[e]	4.14[e]	0.12[e]	0.15[e]
MnO	0.053	0.047	0.006	0.013	0.091	0.005	0.006
MgO	1.447	0.337	0.811	0.377	2.555	0.024	0.034
CaO	2.29	1.72	3.31	1.52	10.34	6.66	8.32
Na_2O	2.18	1.78	1.17	4.10	2.21	2.35	1.78
K_2O	5.208	4.964	3.325	4.376	4.915	0.942	0.904
P_2O_5	0.060	0.040	0.020	0.238	0.233	0.009	0.007
Sr	158	313	154	152	587	29990	4263
Zr	464	565	138	253	174	<2	3
V	116	40	42	331	195	35	32
Cr	40	32	34	39	76	39	34
Total[f]	100.25	99.58	100.13	99.73	99.82	99.91	100.32
LOI[g]	16.14	11.57	13.20	9.41	9.61	15.65	15.70
Al:(Al + Si)	20.5	16.9	16.6	18.5	14.9	25.3	23.9
SCFM[h]	0.95	0.97	0.95	0.97	0.83	0.91	0.89

[a] Values are in wt % for oxides, ppm for elements.

[b] Sample type and location: ZEO105: wairakite, drill hole 66, Wairakei, New Zealand; ZEO106, wairakite, Bandai-atami, Kohriyama, Fukushima, Japan; ZEO107: gismondine, Capo di Bova, Rome, Italy; ZEO108: gismondine, Castel de Decimo, Roma, Lazio, Italy; ZEO109: thomsonite, Elipse Beach, north shore of Lake Superior, Minnesota, USA; ZEO110: thomsonite, North Table Mountain, Golden, Jefferson County, Colorado, USA; ZEO111: scolecite, Hyerabad, India.

[c] Sample identifier used by the National Museum of Natural History of the Smithsonian Institution.

[d] From *Breck* [1974].

[e] All Fe assumed as Fe_2O_3.

[f] Totals are expressed on a volatile-free basis (i.e., elemental abundances determined on sample after measurement of loss on ignition and Sr, Zr, V, and Cr converted to oxides).

[g] Loss on ignition = weight loss after heating sample to 950°C for 1 hour.

[h] SCFM = $SiO_2/(SiO_2 + CaO + FeO + MgO)$ (for oxide abundances in wt %). Where no FeO abundance is available, all Fe is assumed as Fe_2O_3.

[i] Sample type and location: ZEO112: stellerite, Poonah, Maharashtra, India (originally identified as scolecite, a group 5 zeolite); ZEO113: mesolite, Advocate Harbour, Nova Scotia, Canada; ZEO114: mesolite, Cape d'Or, Cumberland County, Nova Scotia, Canada; ZEO115: natrolite, Sao Pedro, Sao Paulo, Brazil; ZEO116: natrolite, Techlovice, Czechoslovakia; ZEO117: chabazite, Christmas, Gila County, Arizona, USA; ZEO118: chabazite, Cape Blomedin, Nova Scotia, Canada.

[j] Sample type and location: ZEO119: laumontite, Great Notch, Essex County, New Jersey, USA; ZEO120: laumontite, Baltimore, Maryland, USA; ZEO121: stilbite, Margaretsville, Nova Scotia, Canada; ZEO122: stilbite, Nova Scotia, Canada; ZEO123: phillipsite, Pine Valley, Eureka County, Nevada, USA; ZEO124: phillipsite, Garbagna, Allesandria, Italy; ZEO125: erionite, Needle Peak, Pershing County, Nevada, USA.

[k] Sample type and location: ZEO126: erionite, Crooked Creek, Rome, Malheur County, Oregon, USA; ZEO127: clinoptilolite, Sheaville, Malheur County, Oregon, USA; ZEO128: clinoptilolite, Fish Creek Mountains, Nevada, USA; ZEO129: mordenite, Trinity Basin, Pershing County, Nevada, USA; ZEO130: mordenite, Crooked Creek, Rome, Malheur County, Oregon, USA; ZEO131: heulandite, Paterson, New Jersey, USA: ZEO132: heulandite, Teigarhorn, Iceland.

either distinct absorption bands or as shoulders superimposed on the short wavelength wing of the O-H stretching fundamental in the 2.8-μm region. Differences are also seen in the number and wavelength positions of resolvable Si-O and Al-O stretching bands in the 10-μm region and the wavelength position of the Christiansen band in the 8-μm region.

4.2. Group 2 Zeolites

[22] Erionite is the only member of this group included in the present study. Compositionally the two samples are consistent with the ideal formula and previous compositional determinations [*Deer et al.*, 1963]. The two erionite spectra are broadly similar to each other as well as to the group 1 zeolites (Figure 1). The longer wavelength bands near 2.8, 6.1, and between 7.7 and 10.1 μm are similar between the two samples, with wavelength positions varying by less than 10 nm. Both erionite samples contain a few percent iron whose oxidation state was not determined. Both spectra exhibit weak absorption bands near 0.66 and 0.92 μm, suggesting that the iron is present in both ferric and ferrous oxidation states. The spectra also exhibit prominent inflections near 0.37 and 0.49 μm, as well as the steep reflectance dropoff shortward of 0.6 μm due to metal-oxygen charge transfers [*Burns*, 1993a, 1993b].

4.3. Group 4 Zeolites

[23] This group is represented by two samples of chabazite in the present study. Compositionally the two

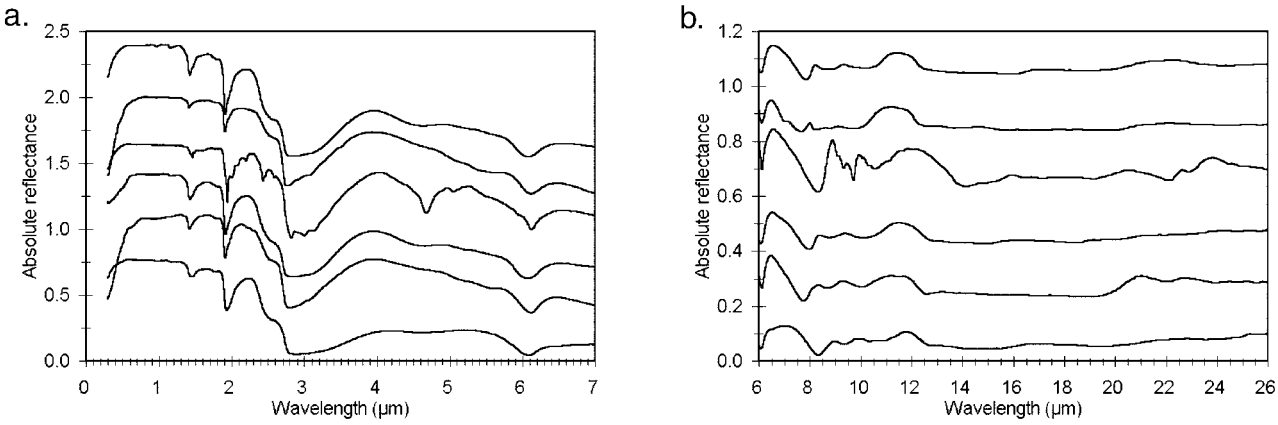

Figure 1. Reflectance spectra of <45 μm grain size fractions of representative zeolites from each structural group. From bottom to top: gismondine (ZEO107; group 1); erionite (ZEO125; group 2); chabazite (ZEO118; group 4); natrolite (ZEO116; group 5); mordenite (ZEO129; group 6); stilbite (ZEO121; group 7): (a) 0.3- to 7-μm spectra with each spectrum vertically offset by +0.3 from the spectrum below it for clarity (no offset for the gismondine). (b) 6- to 26-μm reflectance spectra of the same samples with each spectrum vertically offset by +0.2 from the spectrum below it for clarity (no offset for the gismondine).

samples are consistent with the ideal formula and those of other chabazites [*Deer et al.*, 1963]. The two chabazite reflectance spectra are similar to each other and broadly similar to the other zeolite spectra (Figure 1). Individual absorption bands in the 2.8-μm region are generally unresolved, appearing as a broad region of low reflectance. Absorption bands in the 6.1-, 7.8-, and 10- to 12-μm regions show small differences in wavelength positions between the two spectra. The spectra differ from each other shortward of 1.3 μm probably due to differences in iron content (Table 1). The higher iron sample (ZEO117) has lower overall reflectance, some evidence for weak ferric and ferrous iron absorptions in the 0.7 and 0.9-μm regions, and a steeper dropoff in reflectance shortward of 0.6-μm.

4.4. Group 5 Zeolites

[24] This group is represented by two samples each of thomsonite, mesolite, and natrolite, and one sample of scolecite (ZEO111). The two thomsonites, the scolecite (ZEO111), one of the mesolites (ZEO113), and the two natrolite samples are consistent with their ideal compositions and previous compositional determinations [*Deer et al.*, 1963]. One sample which was originally labeled as scolecite (ZEO112) was analyzed using XRD and was found to consist of stellerite with a small amount of stilbite. This interpretation is consistent with the compositional data, and hence this samples was renamed as stellerite, a group 7 zeolite. One of the mesolites (ZEO114) contains more Na than expected (Table 1). The XRD pattern for this sample is more similar to scolecite than mesolite. This is not unexpected as minor substitution of Na for Ca is common in mesolite [*Deer et al.*, 1963]. It should also be noted that zeolite XRD patterns can vary with changes in volatile content [*Breck*, 1974]. We have chosen to retain the original identity of this sample as mesolite.

[25] Group 5 zeolites, and in particular mesolite, scolecite and natrolite, termed the fibrous zeolites, have been noted by a number of investigators, as possessing transmission spectra which are markedly different from other zeolites [*Milkey*, 1960; *Oinuma and Hayashi*, 1967; *Gottardi and Galli*, 1985]. Group 5 spectra show more complex absorption features than the other groups (Figure 1). The number of resolvable absorption bands in zeolite spectra increases with decreasing openness of the zeolite structure [*Breck*, 1974]. Consequently, the group 5 spectra have the most complex spectra because they have the most compact structures and smallest void spaces.

[26] Natrolite has the most complex spectrum in terms of number of absorption bands (Figure 1) and is similar to natrolite spectra measured by other investigators [e.g., *Grove et al.*, 1992]. This spectral complexity is probably attributable to the higher degree of structural order present in this mineral relative to other group 5 zeolites [*Breck*, 1974]. Water molecules tend to cluster around the Na ions, and the channels in which these clusters reside are small [*Breck*, 1974]. Both effects would tend to lead to more resolved absorption bands as the water molecules are restricted to well-defined local electronic environments. The absorption bands in the 2.8- to 3.2-μm region are better resolved than in other zeolite spectra.

4.5. Group 6 Zeolites

[27] This group is represented by two samples of mordenite in the present study. Compositionally the two samples are consistent with the ideal formula and previous analyses [*Deer et al.*, 1963]. One of the mordenite (ZEO129) spectra is shown in Figure 1. The reflectance spectra of the two mordenite samples are similar to each other beyond 1.3 μm, but differ shortward of 1.3 μm due to differences in iron content and its oxidation state (Table 1). The higher iron sample (ZEO130) has lower overall reflec-

tance and exhibits the iron-related absorption features in the 0.7- and 0.9-μm regions and at 0.37 and 0.49 μm. At longer wavelengths they are broadly similar to the other zeolite spectra.

4.6. Group 7 Zeolites

[28] This group is represented by two samples each of stilbite, clinoptilolite, and heulandite, and one sample of stellerite. All of these samples are consistent with their ideal formulas and previous compositional determinations [*Deer et al.*, 1963]. The reflectance spectrum of a stilbite (ZEO121) is shown in Figure 1.

[29] The group 7 spectra show less diversity than the group 5 spectra. They do not show well-resolved absorption bands in the 2.8-μm region. The H-O-H bending fundamental also shows little variation within this group, varying in wavelength position from 6.11 to 6.15 μm. All of the group 7 spectra exhibit three resolvable absorption features in the 7.5- to 11-μm region. There is more spectral variability in this region, with the wavelength position of the Christiansen band ranging between 7.67 and 7.87 μm. All of the spectra exhibit an absorption feature near 2.55 μm and two partially overlapping absorption bands each in the 1.4 and 1.9-μm regions. A number of the spectra also exhibit absorption bands near 0.97 and 1.16 μm. The spectrum of the most iron-rich sample (ZEO127) has the lowest overall reflectance shortward of 1.3 μm, weak but resolvable ferric and ferrous iron absorption bands in the 0.7 and 0.9-μm regions, and the steepest reflectance dropoff shortward of 0.6 μm.

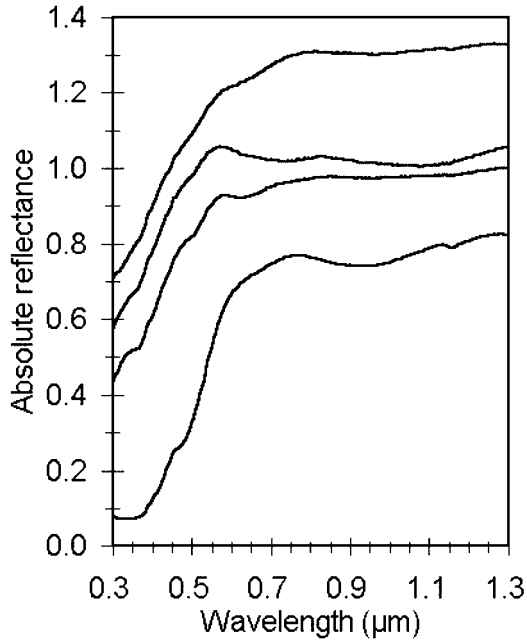

Figure 2. 0.3- to 1.3-μm reflectance spectra of various iron-bearing zeolites showing evidence for iron-related absorption features near 0.37, 0.46, 0.7, and 0.9 μm. Each spectrum has been vertically offset by +0.2 from the one below it for clarity. From bottom to top: phillipsite (group 1; ZEO123); erionite (group 2; ZEO126); mordenite (group 6; ZEO130); clinoptilolite (group 7; ZEO127).

5. Spectral-Compositional-Structural Relationships

[30] Overall, the zeolites included in this study exhibit the same broad types of absorption features; below ~7 μm, the spectra are dominated by absorption features in the 1.4-, 1.9-, 2.5-, 2.8-, and 6.1-μm regions. Longward of this wavelength the spectra are characterized by low overall reflectance and common sets of absorption features in various wavelength regions. In the ensuing discussion, we have grouped spectral features on the basis of the major compositional parameter associated with each.

[31] The absorption features in the zeolite reflectance spectra, particularly beyond ~ 8 μm, are much broader than comparable absorption bands in transmission spectra. This wavelength region is also characterized by low overall reflectance. Thus, the various absorption bands beyond 8 μm are intense, and their broadness results in low overall reflectance and a loss of spectral detail. Similar results were found in a recent comparison of diaspore reflectance and transmission spectra [*Cloutis and Bell*, 2000]. These differences are attributable to the different scattering mechanisms inherent in transmission and reflectance spectroscopy. Results from transmission spectral studies have provided important insights into the causes of various absorption features.

5.1. Iron-Related Spectral Features

[32] A number of the zeolite samples contain a few wt % FeO and/or Fe_2O_3 (Table 1). This results in absorption features near 0.7 and/or 0.9 μm (Figure 2) which are attributable to an Fe^{3+}-Fe^{2+} intervalence charge transfer and an Fe^{2+} crystal field transition, respectively [e.g., *Burns*, 1993a, 1993b]. The high overall reflectance of the spectra allows these bands to be resolved in spite of the relatively low iron contents. The spectra with Fe-associated absorption features also exhibit the steepest reflectance decreases shortward of 0.6 μm, which is attributable to Fe-O charge transfers [*Burns*, 1993a, 1993b].

[33] The spectra of the samples with the highest Fe contents also exhibit weak absorption features near 0.37 and 0.49 μm which are attributed to Fe^{2+} crystal field transitions [*Burns*, 1993a, 1993b]. The presence of iron does not appear to have a systematic effect on the wavelength positions of the various OH-associated absorption features in the 1.4 and 1.9-μm regions, although it is possible that small wavelength shifts in band positions could be offset by structural differences or other cation substitutions. There is an additional absorption feature associated with iron and water at 2.30 μm which is discussed below. Table 2 summarizes the assignments and compositional or structural information associated with the various absorption bands seen in the zeolite spectra.

5.2. Water-Related Spectral Features

[34] A number of investigators have shown that water contained within the voids of the zeolite structure (zeolitic water) is the main contributor to absorption bands associated with H_2O stretching and bending vibrations; OH and adsorbed water are relatively insignificant spectrally

Table 2. Absorption Band Assignments for Zeolites

Wavelength, μm	Assignment	Notes
	Groups 1, 2, 4, 6, and 7 Zeolites and Thomsonite	
0.46	Fe^{2+} crystal field transition	Present in Fe^{2+}-bearing zeolites
~0.7	Fe^{3+}–Fe^{2+} intervalence charge transfer	Present in Fe^{3+}/Fe^{2+}-bearing zeolites
~0.9	Fe^{2+} crystal field transition	Present in Fe^{2+}-bearing zeolites
0.97	Second overtone of H_2O stretch	Present across all classes
1.155–1.160	Symmetric + asymmetric H_2O stretch + H_2O bend (bound water)	Na- and K-rich zeolites
1.160–1.180	Symmetric + asymmetric H_2O stretch + H_2O bend (bound water)	Ca-rich zeolites
1.19	Symmetric + asymmetric H_2O stretch + H_2O bend (adsorbed water)	Present across all classes
1.417–1.422	H_2O stretch + first overtone of H_2O bend (bound water)	Na- and K-rich zeolites
1.424–1.430	H_2O stretch + first overtone of H_2O bend (bound water)	Ca-rich zeolites
~1.47	H_2O stretch + first overtone of H_2O bend (absorbed water)	Present across all classes
1.911	H_2O stretch + bend (bound water)	K-rich zeolites
1.913	H_2O stretch + bend (bound water)	Na-rich zeolites
1.922	H_2O stretch + bend (bound water)	Ca-rich zeolites
~1.970	H_2O stretch + bend (adsorbed water)	Present across all classes
2.30	H_2O stretch + bend (AlFe-OH)	Present across all classes
2.460–2.465	H_2O stretch + bend (AlCa-OH)	Present across all classes
~2.80	H_2O stretch (bound water)	Present across all classes
~3.07	First overtone of H_2O bend (bound water)	Present across all classes
6.05–6.15	H_2O bend (bound water)	Present across all classes
7.50–8.53	Christiansen frequency	Correlated with Al:(Al + Si) ratio
8.3–9.4	Asymmetric Si-O/Al-O stretch	Correlated with Al:(Al + Si) ratio
9.4–10.7	Asymmetric Si-O/Al-O stretch	Correlated with Al:(Al + Si) ratio
11.2–12.1	Transparency peak	Correlated with Al:(Al + Si) ratio
~12.5–15	Symmetric Si-O/Al-O stretch	Some structural group discrimination
~20–26	O-Si-O/O-Al-O bends	Discrimination of group 5 zeolites
	Group 5 Fibrous Zeolites (Water-Related Absorption Bands)	
1.427–1.430	H_2O stretch + first overtone of H_2O bend (Ca-bound water)	Position increases and depth decreases with increasing Na
1.436	H_2O stretch + first overtone of H_2O bend (Ca-bound water)	Only present in scolecite
1.445–1.458	H_2O stretch + first overtone of H_2O bend (Na-bound water)	Position and depth increase with increasing Na
~1.47	H_2O stretch + first overtone of H2O bend (absorbed water)	Partially obscured by other bands
1.485–1.489	H_2O stretch + first overtone of H_2O bend (Ca-bound water)	Position increases and depth decreases with increasing Na
1.940–1.945	H_2O stretch + bend (Ca-bound water)	Depth decreases with increasing Na
~1.970	H_2O stretch + bend (adsorbed water)	Present across all classes
2.005	H_2O stretch + bend (Na-bound water)	Depth increases with increasing Na
2.080	H_2O stretch + bend (Na-bound water)	Depth increases with increasing Na
2.175	H_2O stretch + bend (AlCa-OH)	Depth increases with increasing Ca
2.200	H_2O stretch + bend (AlNa-OH)	Depth increases with increasing Na
2.405	H_2O stretch + bend (AlCa-OH)	Depth increases with increasing Ca
2.430	H_2O stretch + bend (AlNa-OH)	Depth increases with increasing Na
2.465	H_2O stretch + bend (AlCa-OH)	Depth increases with increasing Ca
~2.54	H_2O stretch + bend (AlCa-OH)	Depth increases with increasing Ca
2.590	H_2O stretch + bend (AlNa-OH)	Depth increases with increasing Na
2.790	H_2O stretch (Ca-bound water)	Depth increases with increasing Ca
2.825	H_2O stretch (Na-bound water)	Depth increases with increasing Na
2.925	H_2O stretch (Ca-bound water)	Depth increases with increasing Ca
3.00	H_2O stretch (Na-bound water)	Depth increases with increasing Na
3.09	H_2O stretch (Ca-bound water)	Depth increases with increasing Ca
3.12	H_2O stretch (Na-bound water)	Depth increases with increasing Na
6.01	H_2O bend (Ca-bound water)	Depth increases with increasing Ca
6.03	H_2O bend (Na-bound water)	Depth increases with increasing Na
6.06	H_2O bend (Ca-bound water)	Depth increases with increasing Ca
6.12	H_2O bend (Na-bound water)	Depth increases with increasing Na
6.28	H2O bend (Ca-bound water)	Depth increases with increasing Ca

[*Bertsch and Habgood*, 1963; *Angell and Schaffer*, 1965]. Hence the ensuing discussion relates exclusively to zeolitic water unless otherwise indicated.

5.2.1. 0.97-μm Region

[35] A number of zeolite reflectance spectra exhibit an absorption feature in the 0.97-μm region (Figure 3) [*Hunt and Salisbury*, 1970; *Grove et al.*, 1992]. This feature is attributed to the second overtone of the O-H stretch [*Hunt and Salisbury*, 1970; *Clark et al.*, 1990] and is most evident in the reflectance spectra with high overall reflectance in this region. Its depth is on the order of 2% at most, as expected for a second order overtone. It appears in too few of the zeolite spectra, and is not sufficiently well-resolved in the current data to permit a more detailed analysis. This band may be due to either bound or adsorbed water, as the spectra in this region were not measured under dry conditions.

5.2.2. 1.16-μm Region

[36] A number of the spectra also exhibit an absorption feature near 1.165 μm (Figure 3). This band appears in most of the spectra as a weak (<2% D_b), but distinct, narrow feature. It can be attributed to a combination of a symmetric O-H stretch, an asymmetric O-H stretch and the H-O-H bending fundamental [*Hunt and Salisbury*, 1970; *Clark et*

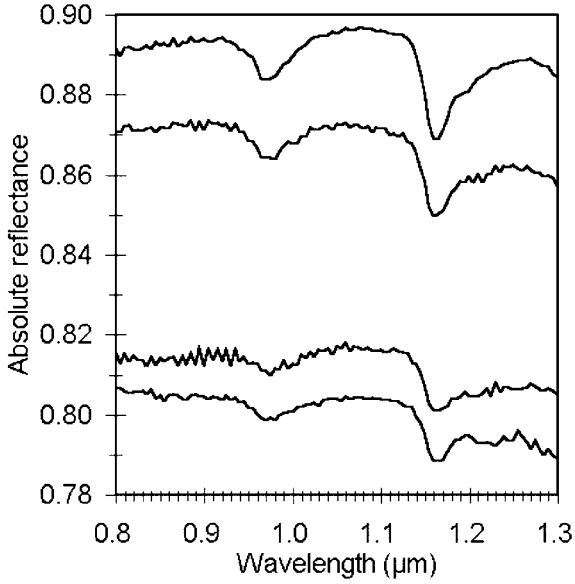

Figure 3. 0.8- to 1.3-μm reflectance spectra of various zeolites showing evidence for H_2O-related absorption features in the 0.97 and 1.16-μm regions. From bottom to top: laumontite (ZEO119; group 1); chabazite (ZEO118; group 4); scolecite (ZEO112; group 5); stilbite (ZEO121; group 7).

al., 1990]. This band is only associated with the presence of water and not OH. It is most commonly found in the spectra of the most volatile-rich zeolites, as expected (groups 1, 2, and 7; Table 1). This feature consists of a strong band in the 1.155- to 1.180-μm region and a weaker shoulder near 1.19 μm. We assign the former to bound water and the latter to adsorbed water, analogous to the results found by *Bishop et al.* [1994] for montmorillonite, where bound water absorption bands occur at shorter wavelengths than adsorbed water absorption bands. The wavelength position of the 1.16-μm band shows some correlation with the major cation present. Its wavelength position generally increases as the major cation weight increases. In Na- and K-rich zeolites, the band occurs between 1.155 and 1.160 μm, while in Ca-rich zeolites it occurs between 1.160 and 1.180 μm. It occurs at generally longer wavelengths in those zeolites with larger voids, consistent with less hydrogen bonding to cations expected in such zeolites (Table 2).

5.2.3. 1.4-μm Region

[37] All of the zeolite spectra exhibit absorption features in the 1.4-μm region. For the majority, this feature consists of a stronger absorption band near 1.42-μm and a weaker band (often appearing as a shoulder) near 1.47 μm (Figure 4). The 1.42-μm band is attributed to bound H_2O combination bands, while the 1.47-μm band is assigned to adsorbed H_2O combination bands [*Bishop et al.*, 1994] because its wavelength position is largely invariant (1.465–1.470 μm). These features involve an H_2O stretch plus the first overtone of the H_2O bend. If group 5 zeolites are ignored, we observe a general increase in the wavelength position of the main

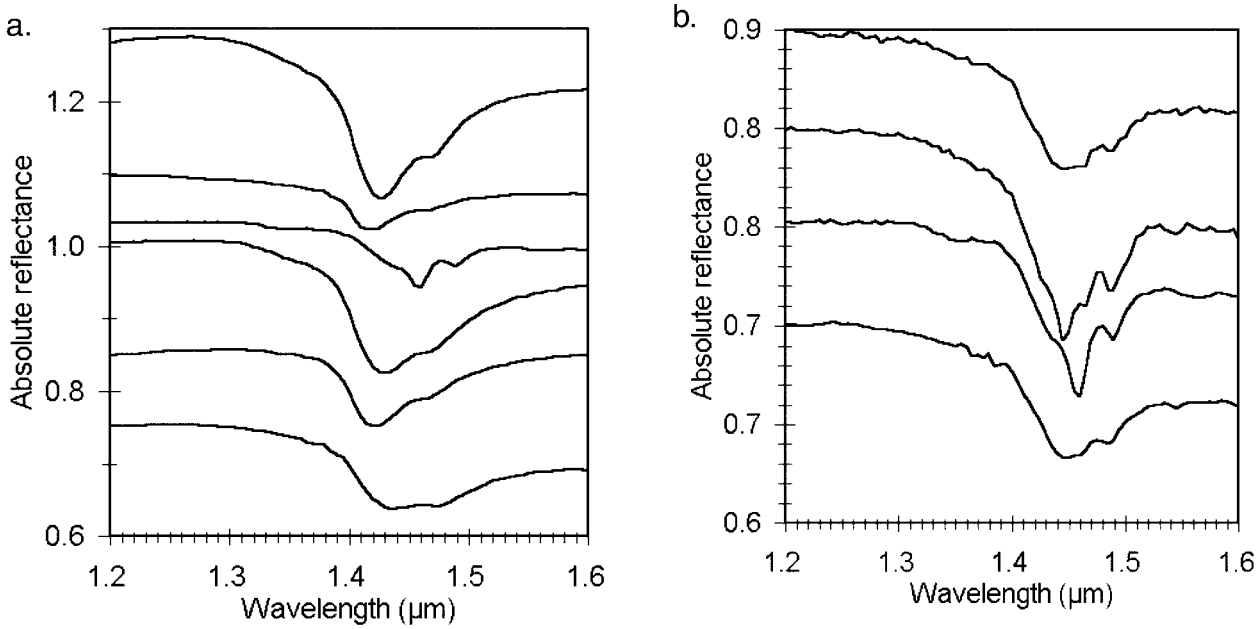

Figure 4. 1.2- to 1.6-μm reflectance spectra of <45-μm grain size fractions of zeolites showing details of absorption features in the 1.4-μm region. Some spectra have been vertically offset by the amount indicated in brackets for clarity. (a) Representative zeolites from each structural group. From bottom to top: gismondine (ZEO107; group 1; no offset); erionite (ZEO125; group 2; +0.05); chabazite (ZEO118; group 4; +0.2); natrolite (ZEO116; group 5; +0.3); mordenite (ZEO129; group 6; +0.3); stilbite (ZEO121; group 7; +0.4). (b) The same for group 5 zeolites; from bottom to top: thomsonite (ZEO109; no offset); natrolite (ZEO116; +0.02); scolecite (ZEO111; +0.06); mesolite (ZEO113; no offset).

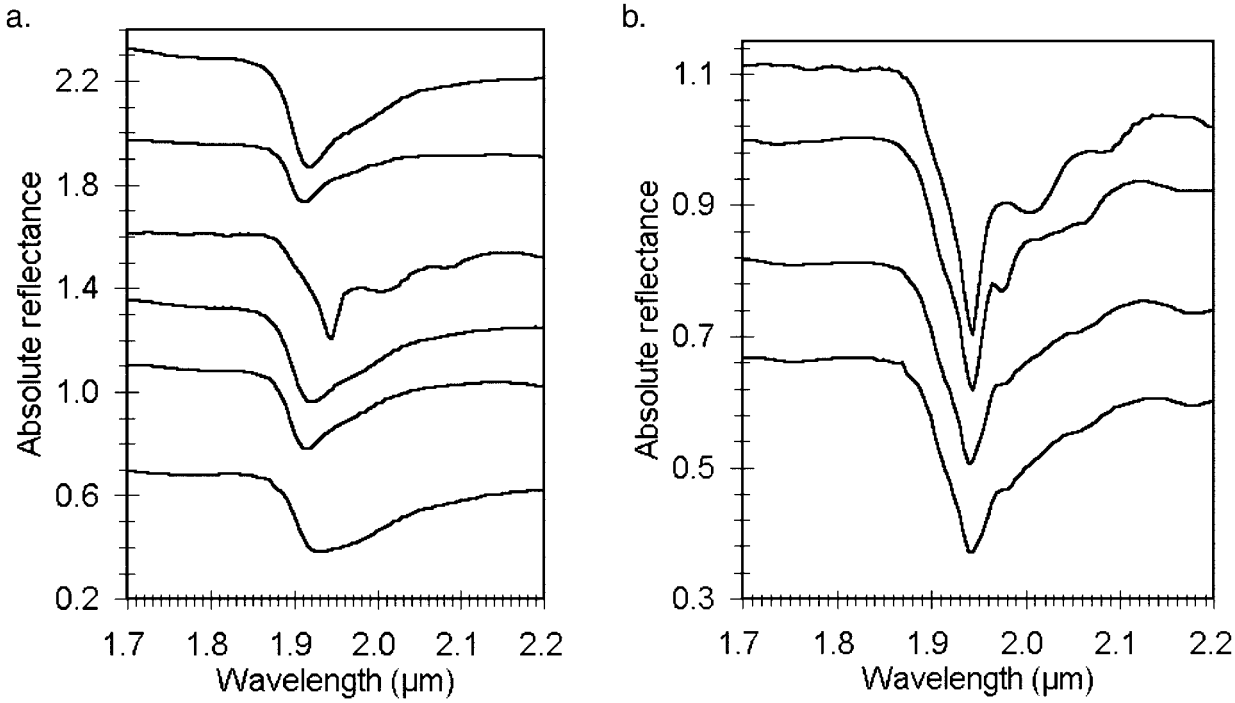

Figure 5. 1.7- to 2.2-μm reflectance spectra of <45-μm grain size fractions of zeolites showing details of absorption features in the 1.9-μm region. (a) Representative zeolites from each structural group. Each spectrum has been vertically offset by +0.3 from the spectrum below it for clarity. From bottom to top: gismondine (ZEO107; group 1; no vertical offset); erionite (ZEO125; group 2); chabazite (ZEO118; group 4); natrolite (ZEO116; group 5); mordenite (ZEO129; group 6); stilbite (ZEO121; group 7). (b) The same for group 5 zeolites (vertical offsets are indicated in brackets); from bottom to top: thomsonite (ZEO109; no offset); mesolite (ZEO113; no offset); scolecite (ZEO111; +0.3); natrolite (ZEO116; +0.4).

absorption band from 1.420 μm in K-bearing zeolites, to 1.422 μm in Na-bearing zeolites to 1.427 μm in Ca-bearing zeolites (Table 2). Thus, the wavelength position of this absorption band can be used to distinguish the major cation present in zeolites. These differences are attributed to the variations in the degree of bonding with the various cations [*Bishop et al.*, 1994]. The different structural groups do not exhibit any systematic trends in terms of positions of these absorption bands.

[38] The group 5 zeolites scolecite, thomsonite, mesolite, and natrolite exhibit more complex absorptions in this wavelength region (Figure 4). Structurally, group 5 zeolites are distinguished from other zeolites by their small channels and clustering of water molecules around the cations. This, coupled with the presence of both Ca and Na in many members of the group (Table 1) should give rise to at least two absorption bands in the 1.4-μm region in addition to the adsorbed water band. This can be seen by comparing the spectra of the scolecite, mesolite, and natrolite (Figure 4). All three are structurally similar with different Na:Ca ratios (Table 1). As Na content increases, the absorption bands in the 1.427- to 1.430- and 1.485- to 1.489-μm regions move to longer wavelengths and decrease in intensity, the bands near 1.436 μm become obscured (present only in the scolecite spectrum), and the band in the 1.445- to 1.458-μm region moves to longer wavelengths and becomes deeper. These results suggest that the 1.436- and 1.445- to 1.458-μm bands are associated with Na-bonded water, while the 1.427- to 1.430- and 1.485- to 1.489-μm bands are associated with Ca-bonded water in these zeolites. It should be noted that the group 5 fibrous zeolites can undergo irreversible dehydration, accompanied by structural rearrangements, and hence the absorption bands in this region are only characteristic of the unaltered minerals.

5.2.4. 1.9-μm Region

[39] Absorption bands in the 1.9-μm region are attributable to a combination of the H_2O stretching and bending modes [*Clark et al.*, 1990; *Bishop et al.*, 1994]. As was the case for the 1.4-μm region, the majority of the zeolite spectra, with the exception of group 5, exhibit a strong absorption band near 1.92 μm and a weaker band near 1.97 μm (Figure 5). The strong band is attributed to bound H_2O combination bands, while the 1.97-μm band is assigned to adsorbed H_2O combination bands [*Bishop et al.*, 1994]. The wavelength position of the band near 1.92-μm ranges from 1.911 to 1.930 μm. The same trends as was observed for the 1.4-μm band is also observed here; i.e., the position of this band generally increases from K-bearing zeolites (1.911 μm average) to Na-bearing zeolites (1.913 μm average) to Ca-bearing zeolites (1.922 μm average) (Table 1). The position of the band near 1.97 μm is largely invariant as would be expected for adsorbed water, ranging between 1.970 and 1.975 μm. It is present in spectra from all the structural groups.

[40] The group 5 fibrous zeolite spectra are more complex in this wavelength region, while thomsonite is similar

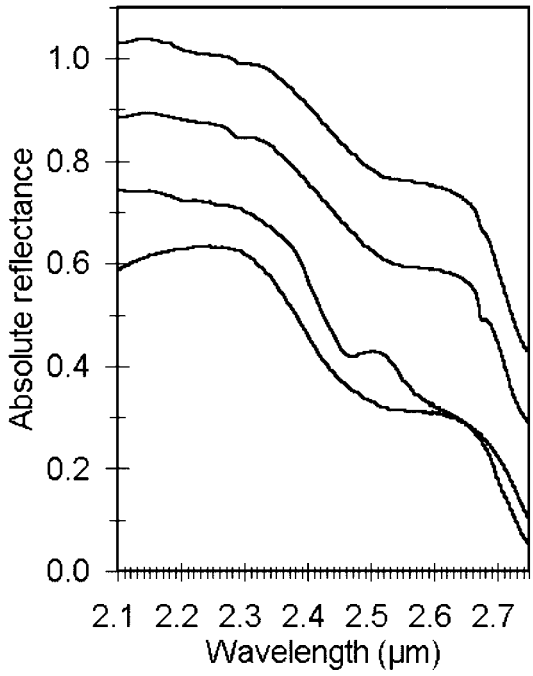

Figure 6. 2.1- to 2.75-μm zeolite reflectance spectra showing details of various cation-H_2O absorption features. Some spectra have been vertically offset by the amount indicated in brackets for clarity. Ca-related absorption band near 2.465 μm is present in gismondine (ZEO108; lower spectrum; no offset) and wairakite (ZEO116; second spectrum from bottom; no offset). An Fe-related absorption band near 2.3 μm is present in clinoptilolite (ZEO127; third spectrum from bottom; +0.2) and erionite (ZEO125; top spectrum; +0.3).

to the other zeolites described above. Scolecite and mesolite are somewhat similar to each other, with well-resolved absorption bands in the 1.940- to 1.945- and 1.975- to 1.977-μm regions, but they also exhibit additional less well-resolved bands at longer wavelengths. Natrolite exhibits the most unique spectrum in this region, with well-resolved absorption bands at 1.942, 2.005, and 2.080 μm (Figure 5) [*Grove et al.*, 1992]. The depth of the band at 1.940–1.945 μm decreases with increasing Na content and there is no clear trend involving band position and Na:Ca ratio. The depths of the bands at 2.005 and 2.080 μm both increase with increasing Na content and are attributed to the Na-water clusters in natrolite [*Breck*, 1974].

5.2.5. 2.1- to 2.5-μm Region

[41] Approximately half of the zeolites in this study exhibit absorption bands in the 2.1- to 2.5-μm region (Figure 6). Absorption band seen in this wavelength region for H_2O/OH-bearing silicates have traditionally been assigned to combinations of the OH stretching and bending vibrations for metal-OH groups. [*Stubičan and Roy*, 1961; *Freund*, 1974; *Moenke*, 1974; *Clark et al.*, 1990]. OH stretching vibrations occur in the 2.8-μm region, while H-O-H librations occur in the 10- to 30-μm region [*Bayly et al.*, 1963; *Ryskin*, 1974], thus absorption bands are expected in the 2.1- to 2.5-μm region due to combinations of these modes, with the wavelength position of the combination bands being a function of the particular cation to which the H_2O is hydrogen bonded. In the case of the current zeolites, the main metals associated with these bands are Ca, Na, K, and Fe. While OH is not expected in zeolites [*Bertsch and Habgood*, 1963], a certain amount of hydrogen bonding can occur between the H_2O hydrogen atoms and the framework oxygen atoms as well as with other cations [*Bertsch and Habgood*, 1963; *Angell and Schaffer*, 1965; *Breck*, 1974; *Ryskin*, 1974]. Three main groups of absorptions were found. The iron-bearing zeolites display a weak absorption feature near 2.30 μm, the Ca-bearing zeolites show an absorption feature near 2.465 μm, and the Na- and K-bearing zeolites display an absorption feature near 2.68 μm. We attribute these features to H_2O stretching plus bending vibrations involving AlFe-OH, AlCa-OH, and Al(Na,K)-OH molecular clusters, respectively. These differences are consistent with the shifts in band positions as a function of a particular cation found by *Bishop et al.* [1994] in montmorillonite spectra.

[42] Once again, the group 5 zeolites exhibit the most complex and numerous absorption features in this wavelength region (Figure 6). On the basis of relative band depths and positions, we assign absorption bands at 2.175, 2.405, and 2.465 μm to AlCa-OH absorptions, as all of these features become more intense as Ca content increases. The bands at 2.175 and 2.465 μm are also seen, weakly, in some of the nonfibrous Ca-rich zeolite spectra, lending further support to these assignments. Bands at 2.200, 2.430, and 2.590 m are probably associated with NaAl-OH absorptions because their intensity increases with Na content.

5.2.6. 2.6- to 3.2-μm Region

[43] Unlike the shorter wavelength regions, the spectra beyond 2.5 μm were measured under dry atmospheric (purged) conditions. Thus, we expect adsorbed water to contribute little if anything to the spectra in this region. The spectral complexity seen at shorter wavelengths, particularly in the 1.4, 1.9, and 2.0- to 2.5-μm regions is mirrored in the 3-μm region. As an example, the group 5 zeolites, which commonly exhibit multiple absorption bands in the 1.4 and 1.9-μm regions, exhibit the greatest number of absorption bands in the 3-μm region (Figure 7).

[44] The 2.6- to 3.2-μm region is characterized in all cases by a series of intense absorption bands. These bands are associated with symmetric and asymmetric O-H stretching vibrations (ν_1 and ν_3) as well as the first overtone of the H-O-H bending fundamental (ν_2) in zeolitic water [*Milkey*, 1960; *Saksena*, 1961; *Bertsch and Habgood*, 1963; *Angell and Schaffer*, 1965; *Oinuma and Hayashi*, 1967; *Moenke*, 1974; *Gottardi and Galli*, 1985; *Tsitsishvili et al.*, 1992]. The number, wavelength position, and intensity of these bands varies as a function of many factors, such as the degree of cation-H_2O or structural oxygen-H_2O bonding, nature of the cations, water content, and electronic environment of the sites occupied by the water molecules [*Bertsch and Habgood*, 1963; *Bayly et al.*, 1963; *Angell and Schaffer*, 1965; *Oinuma and Hayashi*, 1967; *Breck*, 1974; *Ryskin*, 1974]. Differences in transmission spectra in this wavelength region have been used to distinguish different zeolite structural groups [e.g., *Oinuma and Hayashi*, 1967].

[45] All of the reflectance spectra exhibit a broad absorption feature near 2.6 μm, which appears as a prominent

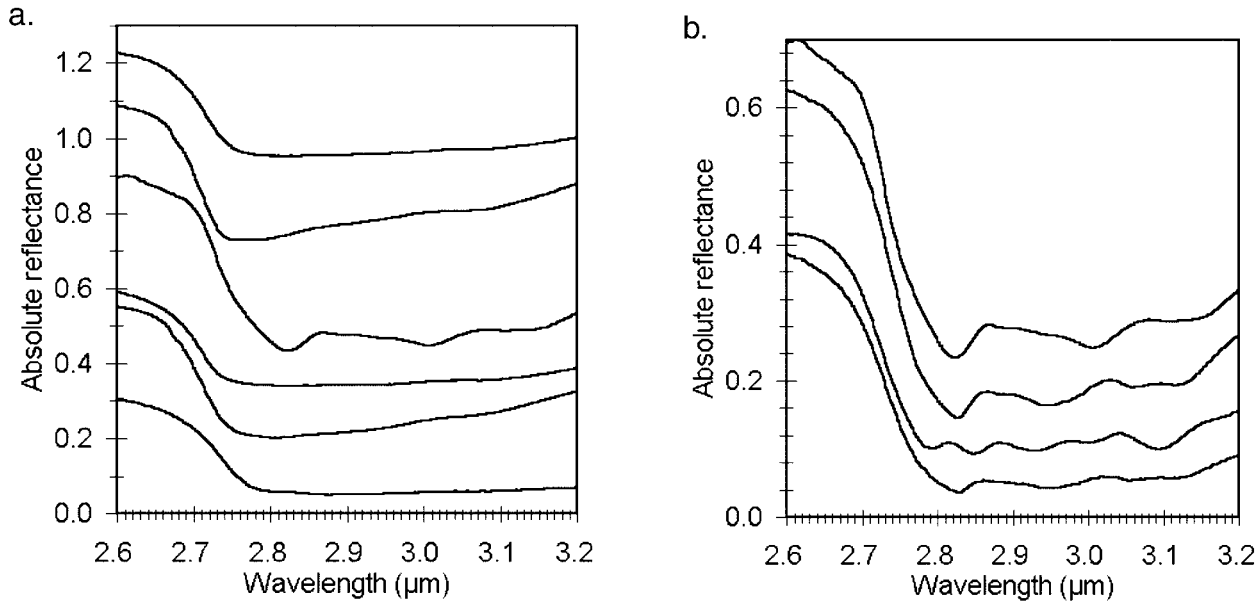

Figure 7. 2.6- to 3.2-μm reflectance spectra of <45-μm grain size fractions of zeolites. Some spectra have been vertically offset by the amount indicated in brackets for clarity. (a) Representative zeolites from each structural group. From bottom to top: gismondine (ZEO107; group 1; no offset); erionite (ZEO125; group 2; +0.1); chabazite (ZEO118; group 4; +0.3); natrolite (ZEO116; group 5; +0.4); mordenite (ZEO129; group 6; +0.6); stilbite (ZEO121; group 7; +0.9). (b) The same for group 5 zeolites. From bottom to top: thomsonite (ZEO109; no offset); scolecite (ZEO111; +0.06); mesolite (ZEO113; +0.1); natrolite (ZEO116; +0.2).

inflection on the short wavelength wing of the fundamental H_2O stretching band (Figure 6). This band is assigned to an asymmetric stretch in H_2O (ν_3) plus the H_2O libration (ν_L) for bound water [*Bayly et al.*, 1963]. An absorption band in this region appears in reflectance spectra of other minerals containing "free" water such as beryl, as well as in H_2O transmission spectra [*Bayly et al.*, 1963; *Clark et al.*, 1990].

[46] Most of the zeolite spectra are characterized by a broad region of intense absorption, with minima near 2.8 and 3.07 μm. These features are assigned to H_2O stretching vibrations and the first overtone of the H_2O bending vibration, respectively [*Bertsch and Habgood*, 1963; *Bayly et al.*, 1963; *Angell and Schaffer*, 1965; *Oinuma and Hayashi*, 1967; *Breck*, 1974; *Ryskin*, 1974; *Clark et al.*, 1990; *Bishop et al.*, 1994]. There is generally insufficient resolution of individual absorption bands in this region to clearly resolve symmetric from asymmetric stretches. Previous investigators have found small differences in terms of the wavelength positions of these bands as a function of cation type and zeolite structural group [*Angell and Schaffer*, 1965] in transmission spectra, with the wavelength position of these bands moving to longer wavelengths as the degree of hydrogen bonding increases [*Oinuma and Hayashi*, 1967]. The current spectra do show a difference in the position of the band near 2.8 μm; it occurs near 2.825 μm in the group 5 spectra, and generally near 2.80 μm in the others. This is consistent with previous interpretations, where hydrogen bonding is greatest in group 5 zeolites [*Tsitsishvili et al.*, 1992]. The intensity and broadness of these absorption features in most of the zeolite reflectance spectra precludes more detailed analysis in terms of correlating small changes in wavelength positions with either structural or compositional variations. Band depths in this region can reach 95% with as little as 10 wt % volatiles (presumed to be water).

[47] The group 5 spectra, once again, show the greatest spectral complexity in this wavelength region (Figure 7) [*Oinuma and Hayashi*, 1967]. They are characterized by a number of absorption features which vary from sample to sample. On the basis of these differences and in conjunction with the other zeolite spectra, we assign the absorption feature at 2.790 and 2.925, and 3.09 μm to Ca-bound H_2O stretching vibrations, and the bands at 2.825 and 3.00, and 3.12 μm to Na-bound H_2O stretching vibrations. The absorption band at 3.09 μm, most prominent in the Ca-rich group 5 spectra, is assigned to the first overtone of the H_2O bending vibration for Ca-rich group 5 zeolites, and the absorption band at 3.00 μm, most prominent in the Na-rich group 5 spectra, is assigned to the first overtone of the H_2O bending vibration for Na-rich group 5 zeolites. As expected given its intermediate composition, the mesolite shows evidence for all of these features. Again, we attribute the multiplicity of bands in the group 5 spectra to the fact that water is highly confined in the channels in these zeolites and can form clusters with the various cations, leading to more discrete energy levels, and hence more resolvable absorption bands [*Breck*, 1974].

5.2.7. 6.1-μm Region

[48] All of the zeolite spectra exhibit an absorption feature near 6.1 μm. This feature is attributed to H-O-H bending vibrations in H_2O (ν_2) [*Clark et al.*, 1990; *Bishop et al.*, 1994]. Given that water is the dominant form of

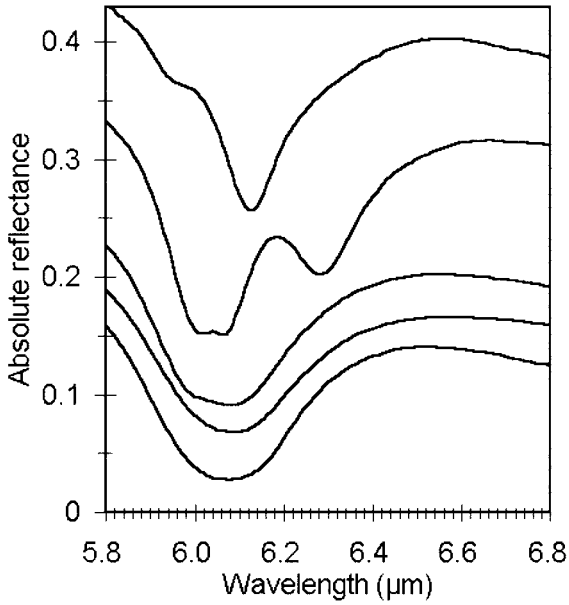

Figure 8. 5.8- to 6.8-μm reflectance spectra of <45-μm grain size fractions of selected zeolites. Some spectra have been vertically offset by the amount indicated in brackets for clarity. From bottom to top: chabazite (ZEO118; group 4; no offset); stilbite (ZEO122; group 7; +0.04); laumontite (ZEO119; group 1; +0.05); scolecite (ZEO111; group 5; +0.1); natrolite (ZEO116; group 5; +0.16).

hydroxyl in zeolites, we see an intense absorption feature in this wavelength region. In the case of the zeolites with only a single absorption band in this region, it occurs at 6.1 ± 0.05 μm (Figure 8). Again, the group 5 spectra exhibit more complex behavior in this region with differences in wavelength positions associated with different cations and degree of hydrogen bonding, but with all bands attributable to H_2O bending vibrations [*Angell and Schaffer*, 1965; *Oinuma and Hayashi*, 1967]. The presence of water molecules in discrete configurations surrounding the various cations in the confined sites and the associated hydrogen bonding leads to complex spectral behavior. The bands at 6.01, 6.06, and 6.28 μm are attributed to Ca-bound H_2O bends, and the bands at 6.03 and 6.12 μm are attributed to Na-bound H_2O bands.

5.2.8. Water Band Summary

[49] As is evident from the water-associated absorption features, the number and position of these bands is a function of a combination of both structure and composition. In the case of zeolites with large void spaces, water-related absorption bands are generally few in number, broad, and relatively constant in wavelength position. In zeolites with small void spaces, hydrogen bonding of water molecules to either cations in the void spaces or oxygens which are part of the aluminosilicate framework is enhanced. The presence of multiple and energetically well-constrained environments for water molecules will lead to multiple and well-resolved water-associated absorption bands.

5.3. Si- and Al-Related Spectral Features

[50] The aluminosilicate framework of zeolites, consisting of different configurations of SiO_4 and AlO_4 tetrahedra, can give rise to absorption features at generally longer wavelengths than those associated with zeolitic water. As was the case with water, such absorption features can be attributed to stretching and bending vibrations whose energy can be mediated by neighboring cations and structural variations which alter the local electronic environment.

5.3.1. 4- to 5-μm Region

[51] A number of the zeolite spectra, and in particular those of group 5, exhibit an absorption feature in the 4.4- to 4.9-μm region (Figure 9). These features are probably the first overtone of the main Si-O stretching vibration present in the 9- to 10-μm region (see below), as changes in the wavelength position and depths of the absorption bands in the 4.4- to 4.9-μm region closely follow those in the 9- to 10-μm region.

5.3.2. Christiansen Frequency

[52] The most intense absorption band is almost always present between 7.50 and 8.53 μm, similar to the reflectance spectra of zeolites measured by other investigators (Figure 9) (e.g., Atmosphere-Surface Turbulent Exchange Facility (ASTER), Web site: http://www.speclib.jpl.nasa.gov, 2000). This band is termed the Christiansen frequency and it occurs where the refractive index of the mineral passes through unity; it is present on the short wavelength wing of an absorption band [*Logan et al.*, 1973; *Salisbury*, 1993]. The wavelength position of the Christiansen frequency is positively correlated with the Al:(Al + Si) ratio (Figure 10) with one exception (ZEO130, mordenite). The higher than expected value for this sample may be due to the intense fundamental band located at longer wavelengths which skews the Christiansen band minimum toward longer wavelengths. This correlation permits the Al:(Al + Si)

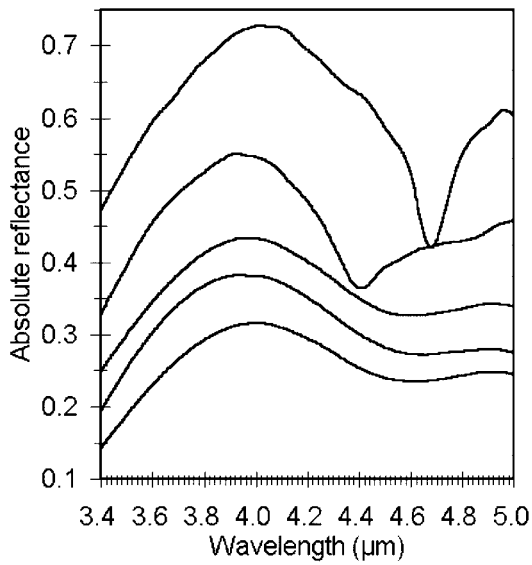

Figure 9. 3.4- to 5.0-μm reflectance spectra of <45-μm grain size fractions of selected zeolites which exhibit resolvable absorption bands in this region. Some spectra have been vertically offset by the amount indicated in brackets for clarity. From bottom to top: stilbite (ZEO122; group 7; no offset); chabazite (ZEO118; group 4; no offset); laumontite (ZEO119; group 1; +0.05); scolecite (ZEO111; group 5; +0.1); natrolite (ZEO116; group 5; +0.2).

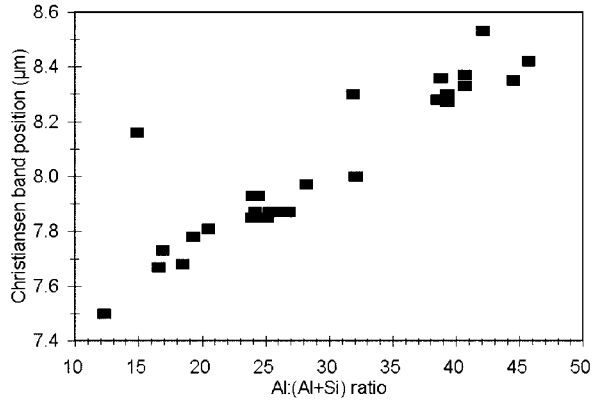

Figure 10. Wavelength position of the Christiansen band in the 7.5- to 8.5-μm region of the zeolite reflectance spectra versus Al:(Al + Si) ratio.

ratio for zeolites to be rapidly constrained from their reflectance spectra. However, it should be noted that the wavelength position of this band can vary as function of viewing geometry, grain size, particle packing, and atmospheric pressure [*Logan et al.*, 1973; *Salisbury and D'Aria*, 1989; *Salisbury and Walter*, 1989], all of which are relatively constant in this study.

[53] The wavelength position of the Christiansen frequency has also been found to be useful for more complex compositional determinations, such as the SCFM index (SiO_2/(SiO_2 + CaO + FeO + MgO)) [*Salisbury and Walter*, 1989]. We found a weak inverse trend between the SCFM index and the wavelength position of the Christiansen band with a fair degree of scatter, similar to the results of *Salisbury and Walter* [1989]. The amount of scatter was much greater than for the Al:(Al + Si) ratio determination. The caveats described above also apply to this determination.

5.3.3. 8.5- to 11-μm Region

[54] Previous transmission spectral studies of zeolites have shown that these minerals exhibit a number of absorption bands in the 8.5- to 11-μm region, which vary among different zeolite structural groups [e.g., *Oinuma and Hayashi*, 1967; *Breck*, 1974]. These bands are attributed to asymmetric O-Si-O and O-Al-O stretching fundamentals (restrahlen bands). However, beyond attributing the most intense of these bands to Si-O stretches, there is generally little agreement on more precise band assignments [*Milkey*, 1960; *Saksena*, 1961; *Stubičan and Roy*, 1961; *Oinuma and Hayashi*, 1967; *Breck*, 1974; *Moenke*, 1974; *Gottardi and Galli*, 1985; *Salisbury and Walter*, 1989; *Tsitsishvili et al.*, 1992]. They are the most intense absorption bands observed in zeolite transmission spectra, and are generally quite broad and few in number [*Milkey*, 1960; *Oinuma and Hayashi*, 1967; *Gottardi and Galli*, 1985]. Spectral differences among zeolites in this wavelength region are expected as the number and wavelength position of these bands will be affected by factors such as Si and Al abundances and structure [e.g., *Milkey* 1960]. Si-Al substitution causes a sufficiently large change in the nature of the stretching vibrations that the wavelength position of the absorption peak in the 9- to 10-μm region in transmission spectra can be correlated with Al:(Al + Si) ratio for many tectosilicates [*Milkey*, 1960]. This peak position ranges from 9.18 m in

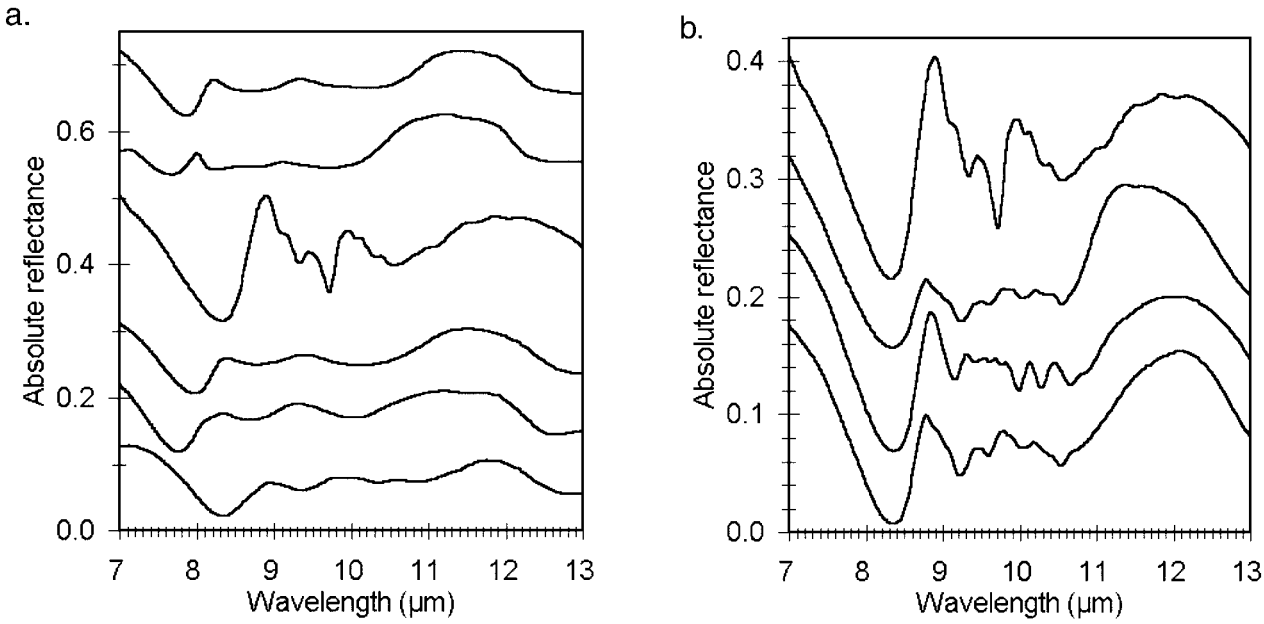

Figure 11. 7- to 13-μm reflectance spectra of <45-μm grain size fractions of zeolites showing details of absorption features in this region. Some spectra have been vertically offset by the amount indicated in brackets for clarity. (a) Representative zeolites from each structural group. From bottom to top: gismondine (ZEO107; group 1; no vertical offset); erionite (ZEO125; group 2; +0.1); chabazite (ZEO118; group 4; +0.2); natrolite (ZEO116; group 5; +0.3); mordenite (ZEO129; group 6; +0.5); stilbite (ZEO121; group 7; +0.6). (b) The same for group 5 zeolites; from bottom to top: thomsonite (ZEO109; no offset); scolecite (ZEO111; +0.06); mesolite (ZEO113; +0.15); natrolite (ZEO116; +0.2).

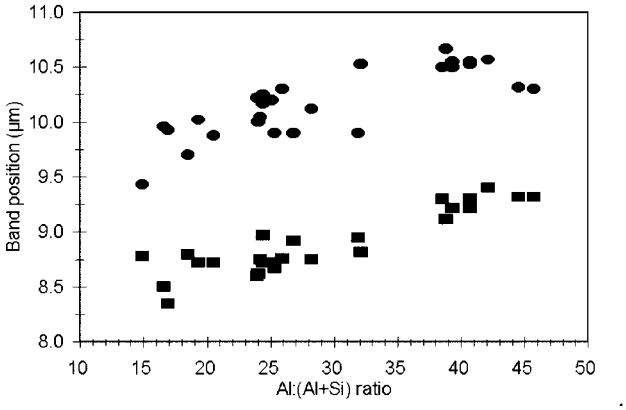

Figure 12. Al:(Al + Si) ratio versus wavelength positions of the two major O-Si-O/ O-Al-O asymmetric stretching fundamentals located in the 8.2- to 9.4-μm (squares) and 9.4- to 10.7-μm (circles) regions of the zeolite reflectance spectra.

quartz (Al:(Al + Si) ratio of 0) to 10.0 μm (Al:(Al + Si) ratio of 0.5). This trend is apparently insensitive to cation substitutions [*Milkey*, 1960].

[55] The 8.5- to 11-μm region of the zeolite reflectance spectra generally show two major absorption bands in the 8.3- to 9.4- and 9.4- to 10.7-μm region (Figure 11). The fibrous zeolite spectra generally exhibit at least 5 bands in this same region. Comparable trends to those found by *Milkey* [1960] were found in our reflectance spectra for both the short (8.3–9.4) and long (9.4–10.7) wavelength bands (Figure 12), indicating that the wavelength positions of these bands in reflectance spectra are useful for constraining Al:(Al + Si) ratios. There is overlap between the different structural groups, suggesting that these band positions are more sensitive to Al:(Al + Si) ratios than structure. However, the positions of these bands is useful for discriminating at least some of the structural groups (Table 3). Within each of the groups there is also a positive correlation between the position of both of these bands and Al:(Al + Si) ratio, with the lower Al content members of each group falling at the lower end of the ranges.

5.3.4. Transparency Peak

[56] The 12-μm region of the reflectance spectra exhibits a reflectance maximum (transparency peak) due to enhanced volume scattering in fine grained materials, and occurs between the Si-O stretching (<12 μm) and bending (>12 μm) vibration bands (Figure 11) [*Salisbury and Walter*, 1989; *Salisbury*, 1993]. These investigators found that the wavelength position of this peak was negatively correlated with SCFM index. The peak is usually only apparent in unpacked powders containing some optically significant fraction of small (<∼45 μm) grains. In the reflectance spectra, the wavelength position of this peak shows a positive correlation with Al:(Al + Si) ratio and a negative correlation with SCFM index (Figure 13). There is appreciably more scatter in the SCFM trend and the three data points which fall appreciably off the trend are all Na-rich samples (natrolite and phillipsite). These data suggest that this feature can be used to constrain Al:(Al + Si) ratio, in most cases generally to within ±5%. As expected, there are no apparent correlations with major cation type or with structural group, since Si and Al contents are the major controls on the position of this feature.

5.3.5. 12.5- to 15-μm Region

[57] Absorption features in the 12.5- to 15-μm range are commonly assigned to symmetric O-Si-O and O-Al-O stretching fundamentals [e.g., *Moenke*, 1974]. These bands are sensitive to Si-Al composition and shift to higher wavelengths with increasing Al content in transmission spectra [*Breck*, 1974]. The reflectance spectra of our samples show a diversity of spectral shapes in this region (Figure 14). This spectral region exhibits between one and three resolvable absorption bands. There is a general trend of increasing band position with increasing Al content but with significant scatter in the data. Many of the spectra exhibit overlapping absorption bands in this region, and using the first resolvable absorption band longward of 12 μm does not fully capture this spectral complexity. The sample spectra whose band positions fall off the general trend exhibit multiple overlapping absorption bands, and prominent inflections are present at the wavelength positions expected on the basis of their Al:(Al + Si) ratios. There are no apparent correlations between structural groups and either the number or relative strengths of absorption bands in this region, with the exception of the group 5 zeolites which exhibit the greatest number of resolvable absorption bands. As was the case with the absorption bands in the 8.5- to 11-μm region, the position of the first major absorption band in the 12- to 15-μm region does provide a means for discriminating some of the structural groups (Table 3) and the lower Al content members of each group fall at the lower end of the ranges.

5.3.6. 15.5- to 18-μm Region

[58] Absorption features in the 15.5- to 18-μm region should be present only in zeolites which contain double ring (D4R and D6R) structures, specifically groups 3 and 4; these features are assigned to O-Si-O and O-Al-O bends

Table 3. Wavelength Range of O-Si-O and O-Al-O Stretching and Bending Fundamentals by Structural Group

Structural Group	Range, μm				
	Asymmetric Stretches				
1	8.8–9.3	9.7–10.3			
2	8.7	9.9–10.0			
4	8.6–8.8	10.0–10.1			
5	9.1–9.4	9.6–9.7	10.0–10.2	10.3–10.35	10.5–10.7
6	8.8	9.4–9.7			
7	8.5–8.8	9.9–10.3			
	Symmetric Stretches				
1	12.60–12.82				
2	12.60–12.63				
4	12.92–12.95				
5	12.50–14.12				
6	12.80				
7	12.50–12.70				
	Bends				
1	23.3–24.5				
2	22				
4	21.8–21.9				
5	21.3–22.1				
6	24.4–24.5				
7	23.8–24.9				

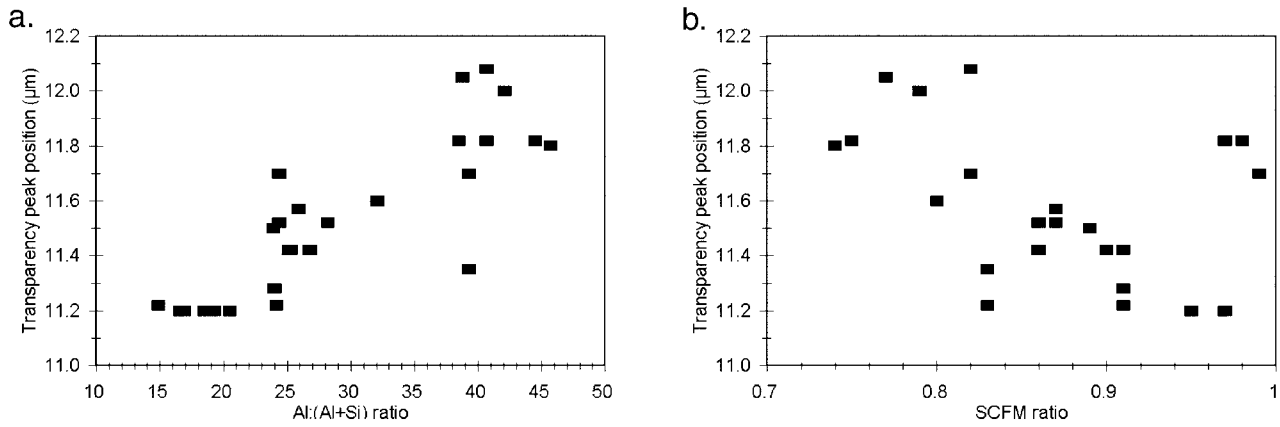

Figure 13. Wavelength position of the transparency peak in the 12-μm region of the zeolite reflectance spectra as a function of composition: (a) versus Al:(Al + Si), (b) versus SCFM index.

[*Breck*, 1974]. Absorption bands in this region are present in a number of transmission and reflectance spectra of zeolites besides those from groups 3 and 4, but are most resolvable in the chabazite spectra (group 4). However, an absorption feature in this region is probably not diagnostic enough to permit its use in reliably discriminating type 3 and 4 zeolites.

5.3.7. 20- to 26-μm Region

[59] Absorption features in the 20- to 26-μm region are largely assigned to O-Si-O and O-Al-O bending vibrations [*Stubičan and Roy*, 1961; *Breck*, 1974; *Moenke*, 1974; *Ryskin*, 1974]. Their wavelength positions are apparently not very sensitive to Si:Al ratios [*Breck*, 1974]. We found no well-defined correlations between wavelength positions of any of the bands in this region and Si:Al ratios. An added complication in searching for trends in this wavelength region is the lack of well-resolved absorption bands in many of the spectra (Figure 15). It was found, however, that the group 5 spectra consistently displayed the strongest absorption band in this region shortward of 22.2 μm, while the remaining spectra exhibited the strongest absorption band longward of 22.2 μm. These differences are probably related to the relative importance of particular bending vibrations for specific zeolite groups. In addition, the

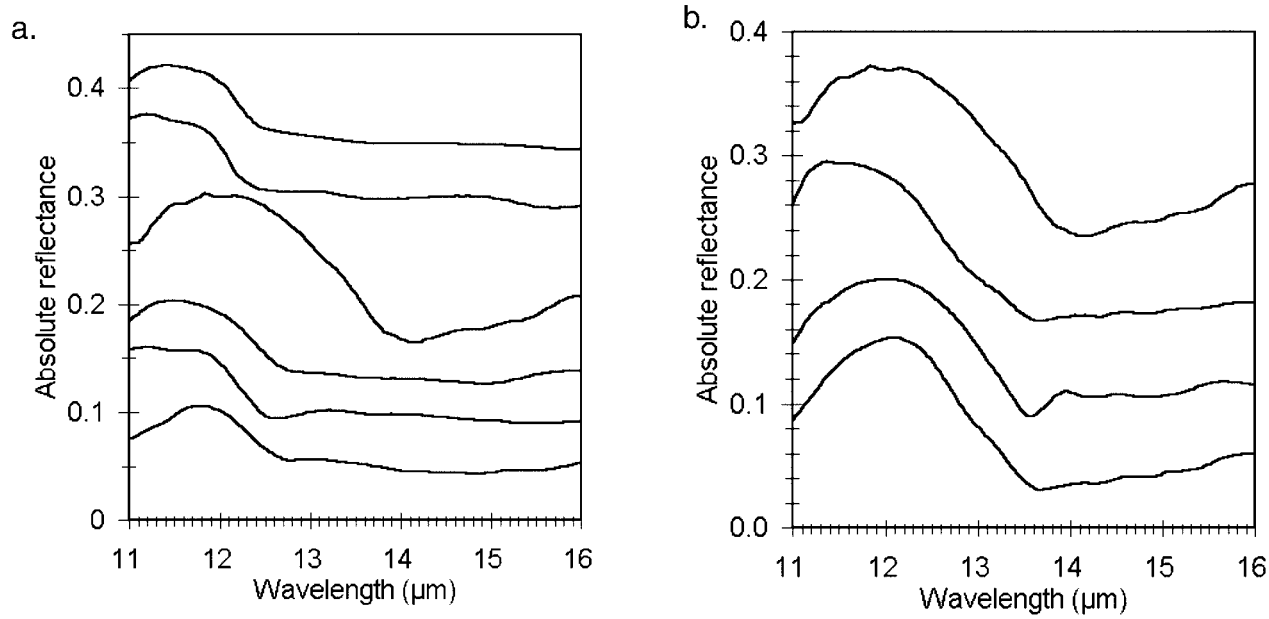

Figure 14. 11- to 16-μm reflectance spectra of <45-μm grain size fractions of zeolites showing details of absorption features in this region. Some spectra have been vertically offset by the amount indicated in brackets for clarity. (a) Representative zeolites from each structural group. From bottom to top: gismondine (ZEO107; group 1; no offset); erionite (ZEO125; group 2; +0.05); chabazite (ZEO118; group 4; +0.1); natrolite (ZEO116; group 5; +0.13); mordenite (ZEO129; group 6; +0.25); stilbite (ZEO121; group 7; +0.3). (b) The same for group 5 zeolites; from bottom to top: thomsonite (ZEO109; no offset); scolecite (ZEO111; +0.06); mesolite (ZEO113; +0.15); natrolite (ZEO116; +0.2).

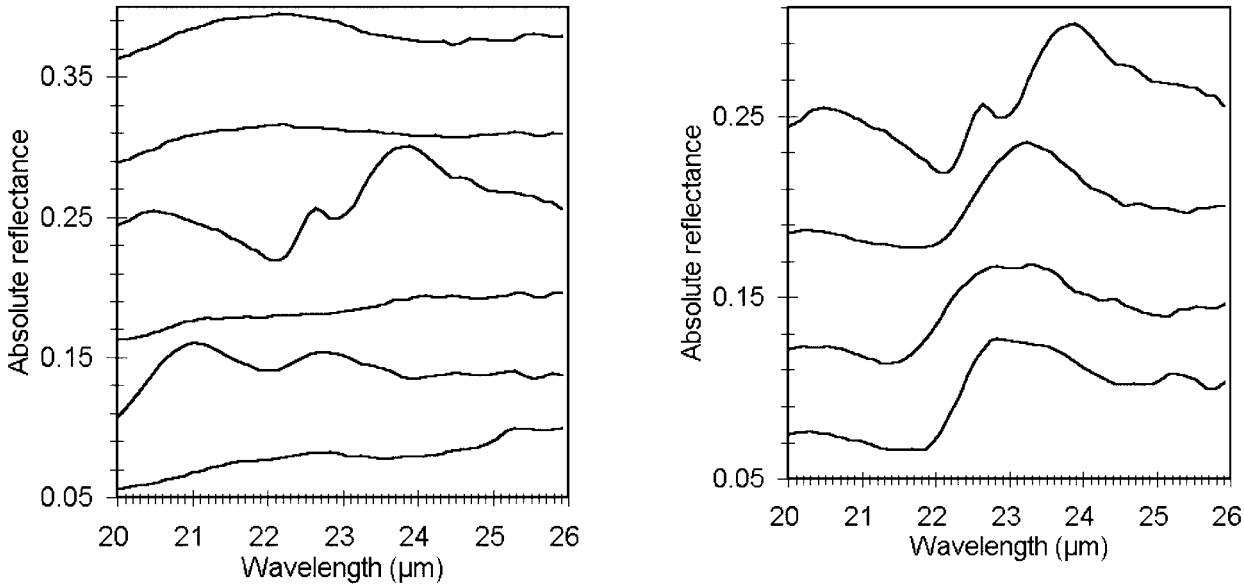

Figure 15. 20- to 26-μm reflectance spectra of <45-μm grain size fractions of zeolites. Some spectra have been vertically offset by the amount indicated in brackets for clarity. (a) Representative zeolites from each structural group. From bottom to top: gismondine (ZEO107; group 1; no offset); erionite (ZEO125; group 2; +0.05); chabazite (ZEO118; group 4; +0.12); natrolite (ZEO116; group 5; +0.16); mordenite (ZEO129; group 6; +0.25); stilbite (ZEO121; group 7; +0.3). (b) The same for group 5 zeolites; from bottom to top: thomsonite (ZEO109; no offset); scolecite (ZEO111; +0.06); mesolite (ZEO113; +0.15); natrolite (ZEO116; +0.16).

position of the first resolvable absorption band longward of 21 μm allows some discrimination of the different structural groups (Table 3).

6. Remote Sensing Implications

[60] Because water is generally not tightly bound in zeolites, has varying abundances, and water content and zeolite structure are often coupled [*Deer et al.*, 1963; *Delgass et al.*, 1969; *Gottardi and Galli*, 1985; *Tsitsishvili et al.*, 1992], zeolite spectra can be quite diverse, unlike most other silicate and aluminosilicate minerals. While the diversity of spectral shapes seen in the wavelength regions associated with H_2O has some promise for analysis of pure phases, the situation is quite different from a remote sensing perspective. Given that zeolite spectra are dominated by H_2O-, Si-, and Al-associated absorption features, their spectra are relatively simple [*Gaffney et al.*, 1984].

[61] The H_2O-associated features can be easily obscured by other H_2O/OH-bearing minerals and many of the metal-OH features in the 2.1- to 2.5-μm region are also found in other mineral spectra [*Clark et al.*, 1990]. The high reflectance of zeolites in the visible and near-infrared wavelength region can easily be reduced, and the absorption bands reduced in intensity, by small quantities of intimately mixed opaque minerals [*Clark*, 1983; *Orenberg and Handy*, 1992]. In this sense they are similar to other common hydrated aluminosilicates such as kaolinite and montmorillonite [e.g., *Clark et al.* 1990].

[62] Other absorption features located below 3.3 μm which might be useful for detection and discrimination of zeolites are associated with the O-H stretching and bending fundamentals, combination, and overtone bands, with the exception of the Fe-associated features seen below 0.9 μm. The main wavelength regions associated with water (1.4, 1.9, and 2.8 μm) are areas where atmospheric water is strongly absorbing, leading to difficulties in obtaining high quality reflectance spectra with good signal-to-noise ratios and high spectral resolution necessary for zeolite detection and discrimination.

[63] In terms of remote sensing detection of zeolites on Mars, one factor which must be considered is that many zeolites undergo structural rearrangements during dehydration which may lead to spectral changes. Zeolites are expected to be readily susceptible to dehydration under current Martian surface conditions [*Gooding*, 1985; *Ming and Gooding*, 1988] and a high priority for our group for the future is to measure the spectra of zeolites under simulated Martian surface conditions [*Craig et al.*, 2001]. This will allow us to assess how zeolite reflectance spectra react to exposure to Martian surface conditions (i.e., simulated temperatures, atmospheric pressure and composition, and ultraviolet light regime). More importantly we will also determine how the more diagnostic Si-O and Al-O bands in the 10-μm region are affected by this exposure, and whether these absorption bands are still useful for zeolite detection and discrimination.

7. Conclusions

[64] The 0.3- to 26-μm reflectance spectra of zeolites are characterized by high overall reflectance and all of the spectra exhibit a number of common absorption features such as H_2O-associated absorption bands in the 1.4-, 1.9-, 2.7- to 3.1-, and 6.1-μm regions, and Si- and Al-associated absorption bands in the 10- to 26-μm region. The shapes and

intensities of these bands are a function of a number of factors, some of which are intimately coupled. These include cation type, void size, and structural properties of the aluminosilicate framework. These in turn cause variations in the local electronic environment which affects properties such as degree of hydrogen bonding and interatomic distances. Such variations are expressed in the reflectance spectra as changes in the number, relative intensities, and wavelength positions of various absorption bands. The relationships between composition, structure, and spectral properties are sufficiently understood to permit discrimination of structural groups, individual zeolites, and identification of major cation types using reflectance spectra. However, in most geological settings, the presence of other minerals in zeolite-bearing assemblages will undoubtedly hinder zeolite detection and discrimination using reflectance spectroscopy.

[65] **Acknowledgments.** The authors wish to thank Janice Bishop for her thorough review of this manuscript and for many helpful suggestions which improved its readability and utility. This study was supported by a research grant from the Natural Sciences and Engineering Research Council of Canada, a contract from the Canadian Space Agency Space Science Program, a discretionary grant from the University of Winnipeg (to E.A.C.), and the Louise McBee Scholarship of the Georgia Association for Women in Education, University of Georgia (to P.M.A.). The authors wish to thank Jeffrey Post, curator-in-charge of the National Museum of Natural History of the Smithsonian Institution, for providing the zeolite samples used in this study, Marilyn Lindstrom and David Mittlefehldt of the NASA Johnson Space Center for analysis of the samples using INAA, Takahiro Hiroi and Carl Pieters of the NASA RELAB spectrometer facility at Brown University for performing the spectral reflectance measurements on the samples, Michael Guertin for his assistance in sample preparation, and Katherine Krenn for assistance in the spectral analysis.

References

Allen, C., J. L. Gooding, and K. Keil, Hydrothermally altered impact melt rock and breccia: Contributions to the soil of Mars, *J. Geophys. Res.*, *87*, 10,083–10,101, 1982.

Alt, J. C., J. Honnorez, C. Laverne, and R. Emmermann, Hydrothermal alteration of a 1 km section through the upper oceanic crust, Deep Sea Drilling Project hole 5048: Mineralogy, chemistry, and evolution of seawater-basalt interactions, *J. Geophys. Res.*, *91*, 10,309–10,335, 1986.

Angell, C. L., and P. C. Schaffer, Infrared spectroscopic investigations of zeolites and adsorbed molecules, 1, Structural OH groups, *J. Phys. Chem.*, *69*, 3463–3470, 1965.

Bargar, K. E., and M. H. Beeson, Hydrothermal alteration in research drill hole Y-2, Lower Geyser Basin, Yellowstone National Park, Wyoming, *Am. Miner.*, *66*, 473–490, 1981.

Bargar, K. E., M. H. Beeson, and E. C. Keith, Zeolites in Yellowstone National Park, *Mineral. Rec.*, *12*, 29–38, 1981.

Barnes, D. A., J. R. Boles, and J. Hickey, Zeolite occurrences in Triassic-Jurassic sedimentary rocks, Baja California Sur, Mexico, in *Proceedings of the Sixth International Zeolite Conference*, 10–15 July 1983, Reno, Nev., pp. 584–594, 1984.

Barrer, R. M., *Hydrothermal Chemistry of Zeolites*, 361 pp., Academic, San Diego, Calif., 1982.

Basu, A., J. Schmitt, and L. Crossey, An argument for zeolites in Mars rocks and an earth analog, *Lunar Planet. Sci. Conf.*, *XXIX*, abstract 1041, 1998.

Bayly, J. G., V. B. Kartha, and W. H. Stevens, The absorption spectra of liquid phase H_2O, HDO and D_2O from 0.7 μm to 10 μm, *Infrared Phys.*, *3*, 211–223, 1963.

Beiersdorfer, R. E., and D. W. Ming, Intensive and bulk compositional controls on hydrothermally altered mafic rocks—Implications on the study of Martian hydrothermal metamorphism, *Lunar Planet. Sci. Conf.*, *XXVII*, 85–86, 1996.

Bell, J. F., III, et al., Mineralogical and compositional properties of Martian soil and dust: Results from Mars Pathfinder, *J. Geophys. Res.*, *105*, 1721–1755, 2000.

Berkley, J. L., Mars weathering analogs: Secondary mineralization in Antarctic basalts, *Proc. Lunar Planet. Sci. Conf.*, *12*, 1481–1492, 1981.

Berkley, J. L., and M. J. Drake, Weathering on Mars: Antarctic analog studies, *Icarus*, *45*, 231–249, 1981.

Bertsch, L., and H. W. Habgood, An infrared spectroscopic study of the adsorption of water and carbon dioxide by Linde Molecular Sieve X, *J. Phys. Chem.*, *67*, 1621–1628, 1963.

Bishop, J. L., C. M. Pieters, and J. O. Edwards, Infrared spectroscopic analyses on the nature of water in montmorillonite, *Clays Clay Miner.*, *6*, 702–716, 1994.

Boles, J., Zeolites in deep-sea sediments, in *Mineralogy and Geology of Natural Zeolites, Reviews in Mineralogy*, vol. 4, edited by F. A. Mumpton, pp. 137–160, Miner. Soc. Am., Washington, D. C., 1981.

Bonatti, E., Palagonite, hyaloclastites and alteration of volcanic glass in the ocean, *Bull. Volcanol.*, *28*, 257–269, 1965.

Bowers, T. S., and R. G. Burns, Activity diagrams for clinoptilolite: Susceptibility of this zeolite to further diagenetic reactions, *Am. Miner.*, *75*, 601–619, 1990.

Breck, D. W., *Zeolite Molecular Sieves*, 766 pp., John Wiley, New York, 1974.

Browne, P. R. L., and A. J. Ellis, The Ohaki-Broadlands hydrothermal area, New Zealand: Mineralogy and related geochemistry, *Am. J. Sci.*, *269*, 759–763, 1970.

Browne, P. R. L., S. F. Courtney, and C. P. Wood, Formation rates of calc-silicate minerals deposited inside drillhole casing, Ngatamariki geothermal field, New Zealand, *Am. Miner.*, *74*, 759–763, 1989.

Burns, R. G., Origin of electronic spectra of minerals in the visible to near-infrared region, in *Remote Geochemical Analysis: Elemental and Mineralogical Composition*, edited by C. M. Pieters and P. A. J. Englert, pp. 3–29, Cambridge Univ. Press, New York, 1993a.

Burns, R. G., *Mineralogical Applications of Crystal Field Theory*, 2nd ed., Cambridge Univ. Press, New York, 1993b.

Carr, M. H., *Water on Mars*, Oxford Univ. Press, New York, 1996.

Clark, R. N., Spectral properties of mixtures of montmorillonite and dark carbon grains: Implications for remote sensing minerals containing chemically and physically adsorbed water, *J. Geophys. Res.*, *88*, 10,635–10,644, 1983.

Clark, R. N., and T. L. Roush, Reflectance spectroscopy: Quantitative analysis techniques for remote sensing applications, *J. Geophys. Res.*, *89*, 6329–6340, 1984.

Clark, R. N., T. V. V. King, M. Klejwa, G. A. Swayze, and N. Vergo, High spectral resolution reflectance spectroscopy of minerals, *J. Geophys. Res.*, *95*, 12,653–12,680, 1990.

Cloutis, E. A., and J. F. Bell III, Diaspores and related hydroxides: Spectral-compositional properties and implications for Mars, *J. Geophys. Res.*, *105*, 7053–7070, 2000.

Coombs, D. S., A. J. Ellis, W. S. Fyfe, and A. M. Taylor, The zeolite facies, with comments on the interpretation of hydrothermal syntheses, *Geochim. Cosmochim. Acta*, *17*, 53–107, 1959.

Craig, M., E. A. Cloutis, and T. Mueller, ME and mini-ME: Two Mars environmental simulation chambers for reflectance spectroscopy, *Lunar Planet. Sci. Conf*, *XXXII*, abstract 1368, 2001.

Deer, W. A., R. A. Howie, and J. Zussman, *Rock Forming Minerals, Framework Silicates*, vol. 4, Copp Clark, Mississauga, Ont., 1963.

Delgass, W. N., R. L. Garten, and M. Boudart, Dehydration and adsorbate interactions of Fe-Y zeolite by Mössbauer spectroscopy, *J. Phys. Chem.*, *73*, 2970–2979, 1969.

Donahoe, R. J., and J. G. Liou, An experimental study on the process of zeolite formation, *Geochim. Cosmochim. Acta*, *49*, 2349–2360, 1985.

Feins, I. R., and P. A. Mullen, Diffuse reflectance spectra of rare earth exchanged synthetic zeolites in the visible region, *Am. Chem. Soc., Div. Pet. Chem., Prepr.*, *15*, A89–A97, 1970.

Foord, E. E., H. C. Starkey, and J. E. Taggart Jr., Mineralogy and paragenesis of "pocket" clays and associated minerals in complex granitic pegmatites, San Diego County, California, *Am. Miner.*, *71*, 428–439, 1986.

Freund, F., Ceramics and thermal transformations of minerals, in *The Infrared Spectra of Minerals*, edited by V. C. Farmer, pp. 465–482, Mineral. Soc., London, UK, 1974.

Gaffney, E. S., R. B. Singer, and T. D. Kunkie, Zeolites on Mars: Prospects for remote sensing, in *Reports of the Planetary Geology and Geophysics Program 1984*, NASA, Washington, D. C., 397, 1984.

Geptner, A. R., Palagonite and the process of palagonitization, *Lithol. Miner. Resour.*, *5*, 594–607, 1970.

Gibson, E. K., Jr., Sources and sinks of present day water within the Martian regolith: Evidence from a terrestrial analog of Martian weathering processes—the dry valleys of Antarctica, *Workshop on Water on Mars*, *LPI Tech. Rep. 85-03*, pp. 26–28, Lunar Planet. Inst., Houston, Tex., 1985.

Gibson, E. K., S. J. Wentworth, and D. S. McKay, Chemical weathering and diagenesis of a cold desert soil from Wright Valley, Antarctica: An analog of Martian weathering processes, *Proc. Lunar Planet. Sci., 13th*, Part I, *J. Geophys. Res.*, *88*, suppl., A912–A928, 1983.

Golden, D. C., D. W. Ming, R. V. Morris, and H. V. Lauer Jr., Mars surface weathering products and spectral analogs: Palagonites and synthetic iron minerals, *Workshop on the Martian Surface and Atmosphere Through Time*, *LPI Tech. Rep. 92-02*, pp. 59–60, 1992.

Gooding, J. L., Low temperature aqueous alteration in the early solar system: Possible clues from meteorites weathered in Antarctica, *Lunar Planet. Sci. Conf.*, *XV*, 308–309, 1984a.

Gooding, J. L., Search for "Martian (?) weathering" effects in achondrites EETA79001 and ALHA77005, *Lunar Planet. Sci. Conf.*, *XV*, 310–311, 1984b.

Gooding, J. L., Water and ice in the Martian regolith: Dependence of stabilities on regolith mineralogy, *Workshop on Water on Mars*, *LPI Tech. Rep. 85-03*, pp. 29–31, Lunar Planet. Inst., Houston, Tex., 1985.

Gooding, J. L., Martian dust particles as condensation nuclei: A preliminary assessment of mineralogical factor, *Icarus*, *66*, 56–74, 1986.

Gottardi, G., and E. Galli, *Natural Zeolites*, 393 pp., Springer-Verlag, New York, 1985.

Grove, C. I., S. J. Hook, and E. D. Paylor II, *Laboratory Reflectance Spectra of 160 Minerals, 0.4 to 2.5 Micrometers, JPL Publ. 92-2*, Jet Propul. Lab., Pasadena, Calif., 1992.

Hay, R. L., and A. Iijima, Nature and origin of palagonitic tuffs of the Honolulu Group on Oahu, Hawaii, *Mem. Geol. Soc. Am.*, *116*, 331–376, 1968.

Honda, S., and L. P. J. Muffler, Hydrothermal alteration in core from research drill hole Y-1, Upper Geyser Basin, Yellowstone National Park, Wyoming, *Am. Miner.*, *55*, 1714–1737, 1970.

Hunt, G. R., and J. W. Salisbury, Visible and near infrared spectra of minerals and rocks, 1, Silicate minerals, *Mod. Geol.*, *1*, 283–300, 1970.

Iijima, A., K. Aoyagi, and T. Kazama, Diagenetic zeolite zone modified by recent high heat flow in Miti-KuromatSunai hole, southwest Hokkaido, Japan (geothermally modified zeolite zone), in *Proceedings of the Sixth International Zeolite Conference*, 10–15 July, 1983, Reno, Nev., pp. 595–603, 1984.

Jakes, P. J., and D. Rajmon, Zeolites—Fate of Martian water?, *Lunar Planet. Sci. Conf.*, *XXIX*, 1627, 1998.

Jercinovic, M. J., K. Keil, M. R. Smith, and R. A. Schmitt, Alteration of basaltic glass from north-central British Columbia, Canada, *Geochim. Cosmochim. Acta*, *54*, 2679–2696, 1990.

Johnsson, M. J., Overlooked sedimentary particles from tropical weathering environments, *Geology*, *18*, 107–110, 1990.

Johnson, J. R., et al., Preliminary results on photometric properties of materials at the Sagan Memorial Station, Mars, *J. Geophys. Res.*, *104*, 8809–8830, 1999.

Kristmannsdottir, H, and J. Tomasson, Zeolite zones in geothermal areas in Iceland, in *Natural Zeolites: Occurrence, Properties, Use*, edited by L. B. Sand and F. A. Mumpton, pp. 277–284, Pergamon, new York, 1978.

Logan, L. M., G. R. Hunt, J. W. Salisbury, and S. R. Balsamo, Compositional implications of Christiansen frequency maximums for infrared remote sensing applications, *J. Geophys. Res.*, *78*, 4983–5003, 1973.

Luhr, J. F., and T. K. Kyser, Primary igneous analcime: The Colima minettes, *Am. Miner.*, *74*, 216–223, 1989.

McCulloh, T. H., V. A. Frizzell, R. J. Stewart, and I. Barnes, Precipitation of laumontite with quartz, thenardite, and gypsum at Sepse Hot Springs, Western Transverse Ranges, California, *Clays Clay Miner.*, *29*, 353–364, 1981.

McSween, H. Y., Jr., and S. L. Murchie, Rocks at the Mars Pathfinder landing site, *Am. Sci.*, *87*, 36–45, 1999.

McSween, H. Y., Jr., et al., Chemical, multispectral, and textural constraints on the composition and origin of rocks at the Mars Pathfinder landing site, *J. Geophys. Res.*, *104*, 8679–8715, 1999.

Mertzman, S. A., K-Ar results from the southern Oregon-northern California Cascade Range, *Oreg. Geol.*, *62*, 99–122, 2000.

Milkey, R. G., Infrared spectra of some tectosilicates, *Am. Miner.*, *45*, 990–1007, 1960.

Ming, D. W., and J. L. Gooding, Zeolites on Mars: Possible environmental indicators in soils and sediments, in *Workshop on Mars Sample Return Science*, pp. 124–125, Lunar Planet. Inst., Houston, Tex., 1988.

Moenke, H. H. W., Silica, the three-dimensional silicates, borosilicates, and beryllium silicates, in *The Infrared Spectra of Minerals*, edited by V. C. Farmer, pp. 365–382, Mineral. Soc., London, UK, 1974.

Oinuma, K., and H. Hayashi, Infrared absorption spectra of some zeolites from Japan, *J. Toyo Univ., Gen. Educ. Nat. Sci.*, *8*, 1–12, 1967.

Orenberg, J., and J. Handy, Reflectance spectroscopy of palagonite and iron-rich montmorillonite clay mixtures: Implications for the surface composition of Mars, *Icarus*, *96*, 219–225, 1992.

Pieters, C. M., Strength of mineral absorption features in the transmitted component of near-infrared light: First results from RELAB, *J. Geophys. Res.*, *88*, 9534–9544, 1983.

Reichen, L. E., and J. J. Fahey, An improved method for the determination of FeO in rocks and minerals including garnet, *U.S. Geol. Surv. Bull.*, *1144B*, 1–5, 1962.

Reflectance Experiment Laboratory (RELAB), *Reflectance Experiment Laboratory (RELAB) Description and User's Manual*, Brown Univ., Providence, R. I., 1996.

Ryskin, Y. I., The vibrations of protons in minerals: hydroxyl, water and ammonium, in *The Infrared Spectra of Minerals*, edited by V. C. Farmer, pp. 137–181, Mineral. Soc., London, UK, 1974.

Saksena, B. D., Infra-red absorption studies of some silicate structures, *Trans. Faraday Soc.*, *57*, 242–255, 1961.

Salisbury, J. W., Mid-infrared spectroscopy: Laboratory data, in *Remote Geochemical Analysis: Elemental and Mineralogical Composition*, edited by C. M. Pieters and P. A. J. Englert, pp. 79–98, Cambridge Univ. Press, New York, 1993.

Salisbury, J. W., and D. D'Aria, Measurement of Christiansen frequencies in spectra of particulate samples for determination of rock composition, *Lunar Planet. Sci. Conf.*, *XX*, 940–941, 1989.

Salisbury, J. W., and L. S. Walter, Thermal infrared (2.5–13.5 μm) spectroscopic remote sensing of igneous rock types on particulate planetary surfaces, *J. Geophys. Res.*, *94*, 9192–9202, 1989.

Sand, L. B., and F. A. Mumpton (Eds.), *Natural Zeolites. Occurrence, Properties, Use*, 545 pp., Pergamon, New York, 1978.

Seki, Y., H. Onuki, K. Okumura, and I. Takashima, Zeolite distribution in Katayama geothermal area, Onikobe, Japan, *Jpn. J. Geol. Geogr.*, *40*, 63–79, 1969.

Staudigel, H., and S. R. Hart, Alteration of basaltic glass: Mechanisms and significance for the oceanic crust-seawater budget, *Geochim. Cosmochim. Acta*, *47*, 337–350, 1983.

Steiner, A., Hydrothermal rock alteration at Wairakei, New Zealand, *Econ. Geol.*, *48*, 1–13, 1953.

Stoiber, R. E., and E. S. Davidson, Amygdule mineral zoning in the Portage Lake lava series, Michigan copper district, *Econ. Geol.*, *54*, 1250–1277, 1959.

Stubičan, V., and R. Roy, Isomorphous substitution and infrared spectra of the layer lattice silicates, *Am. Miner.*, *46*, 32–51, 1961.

Tsitsishvili, G. V., T. G. Andronikashvili, G. N. Kirov, and L. D. Filizova, *Natural Zeolites*, 297 pp., Ellis Horwood, Chichester, England, 1992.

Zamarreno, I., F. Plana, A. Vazquez, and D. A. Clague, Motukoreaite: A common alteration product in submarine basalts, *Am. Miner.*, *74*, 1054–1058, 1989.

Zen, E.-A., The zeolite facies: An interpretation, *Am J. Sci.*, *259*, 401–409, 1961.

Zhou, Z., and W. S. Fyfe, Palagonitization of basaltic glass from DSDP Site 335, Leg 37: Textures, chemical composition, and mechanisms of formation, *Am. Miner.*, *74*, 1045–1053, 1989.

P. M. Asher, Department of Geology and Geography, Georgia Southern University, P.O. Box 8149, Statesboro, GA 30460-8149, USA.

E. Cloutis, Department of Geography, University of Winnipeg, 515 Portage Avenue, Winnipeg, Manitoba, Canada R3B 2E9. (e.cloutis@uwinnipeg.ca)

S. A. Mertzman, Department of Geosciences, Franklin and Marshall College, P.O. Box 3003, Lancaster, PA 17604-3003, USA.